THE JOURNAL OF BIOLOGICAL CHEMISTRY VOL. 291, NO. 26, pp. 13634–13648, June 24, 2016

Type 2 Diabetes Dysregulates Glucose Metabolism in Cardiac Progenitor Cells*[S]

Received for publication, February 17, 2016, and in revised form, April 27, 2016 Published, JBC Papers in Press, May 5, 2016, DOI 10.1074/jbc.M116.722496

Joshua K. Salabei[‡§1], Pawel K. Lorkiewicz[‡§1], Parul Mehra[‡§1], Andrew A. Gibb[‡§¶], Petra Haberzettl[‡§], Kyung U. Hong[‡§], Xiaoli Wei[‖], Xiang Zhang[‖**‡‡], Qianhong Li[‡], Marcin Wysoczynski[‡§], Roberto Bolli[‡§¶], Aruni Bhatnagar[‡§¶§§], and Bradford G. Hill[‡§¶§§2]**

From the [‡]Institute of Molecular Cardiology, [§]Diabetes and Obesity Center, the Departments of [§§]Biochemistry and Molecular Genetics, [¶]Physiology, [‖]Chemistry, [‡‡]Pharmacology and Toxicology, and the [**]Center for Regulatory and Environmental Analytical Metabolomics, University of Louisville, Louisville, Kentucky 40202

Type 2 diabetes is associated with increased mortality and progression to heart failure. Recent studies suggest that diabetes also impairs reparative responses after cell therapy. In this study, we examined potential mechanisms by which diabetes affects cardiac progenitor cells (CPCs). CPCs isolated from the diabetic heart showed diminished proliferation, a propensity for cell death, and a pro-adipogenic phenotype. The diabetic CPCs were insulin-resistant, and they showed higher energetic reliance on glycolysis, which was associated with up-regulation of the pro-glycolytic enzyme 6-phosphofructo-2-kinase/fructose-2,6-bisphosphatase 3 (PFKFB3). In WT CPCs, expression of a mutant form of PFKFB, which mimics PFKFB3 activity and increases glycolytic rate, was sufficient to phenocopy the mitochondrial and proliferative deficiencies found in diabetic cells. Consistent with activation of phosphofructokinase in diabetic cells, stable isotope carbon tracing in diabetic CPCs showed dysregulation of the pentose phosphate and glycero(phospho)lipid synthesis pathways. We describe diabetes-induced dysregulation of carbon partitioning using stable isotope metabolomics-based coupling quotients, which relate relative flux values between metabolic pathways. These findings suggest that diabetes causes an imbalance in glucose carbon allocation by uncoupling biosynthetic pathway activity, which could diminish the efficacy of CPCs for myocardial repair.

Cell therapy is a promising treatment for restoring cardiac function in heart failure patients. Transplantation of cells of diverse origin, including cardiac progenitor cells (CPCs),[3] after myocardial infarction improves left ventricular ejection fraction, diminishes scar size, and retains or increases viable tissue (1–6). In rodent models of diffuse myocardial damage, endogenous CPCs have been suggested to restore cardiac function by regenerating cardiac myocytes (7). In contrast, the results of lineage tracing studies indicate minimal contribution of endogenous CPCs to the production of new cardiac myocytes, although CPC-mediated angiogenesis was observed (8). Despite these inconsistencies, results from several independent laboratories show that transplantation of exogenous CPCs into the damaged heart promotes significant myocardial recovery in several species (9–14). Nevertheless, it remains unclear how transplanted cells promote myocardial recovery, whether the benefits of cell therapy have been maximized, and whether cell therapy is effective for all heart failure patients. Preclinical research is thus required to identify mechanisms that regulate CPC biology and to assess how comorbid conditions affect outcomes of cell therapy.

One critical issue is metabolic disease. In the United States, most heart failure patients are overweight, and up to 65% have diabetes (15–17). This is significant because diabetes inhibits the ability of CPCs (18, 19), as well as other stem/progenitor cells such as endothelial progenitor cells, mesenchymal stem cells, and hematopoietic stem cells, to migrate, proliferate, secrete paracrine factors, differentiate, and/or engraft (20–28). Thus, understanding the mechanisms by which transplanted cells improve cardiac function and how diabetes affects cell therapy could provide a new framework for improving the reparative properties of transplanted cells.

Although it is known that diabetes inhibits cell therapy-mediated tissue repair in numerous contexts, the reasons for diabetes-induced loss of cell competence remain poorly understood. Accordingly, the purpose of this study was to examine how diabetes damages cells commonly isolated for cardiac transplantation. Our results show that diabetes persistently decreases the ability of isolated cells to proliferate, survive oxidative insults, and differentiate, which can be explained at least in part by an uncoupling of biosynthetic glucose metabolism pathways. In addition, we define a novel method for relating changes in flux between different metabolic pathways in the

* This work was supported by National Institutes of Health Grants GM103492 (to A. B.), HL55477 (to A. B.), HL78825 (to R. B.), HL113530 (to R. B.), and HL122580 (to B. G. H.) and the American Diabetes Association Pathway to Stop Diabetes Grant 1-16-JDF-041 (to B. G. H.). Seahorse Bioscience provided travel awards to J. K. S. and B. G. H. for presenting data at scientific meetings but did not contribute to the work described in this manuscript.

[S] This article contains supplemental Tables S1–S3.

[1] These authors contributed equally to this work.

[2] To whom correspondence should be addressed: Dept. of Medicine, Institute of Molecular Cardiology, Diabetes and Obesity Center, University of Louisville, 580 S. Preston St., Rm. 321E, Louisville, KY 40202. Tel.: 502-852-1015; Fax: 502-852-3663; E-mail: bradford.hill@louisville.edu.

[3] The abbreviations used are: CPC, cardiac progenitor cell; DHAP, dihydroxyacetone phosphage; ECAR, extracellular acidification rate; F6P, fructose-6-phosphate; GAP, glyceraldehyde-3-phosphate; GLP, glycerolipid synthesis pathway; pd-PFK2, phosphatase-deficient phosphofructokinase 2; PFK1, phosphofructokinase 1; PFK2, phosphofructokinase 2 (also denoted 6-phosphofructo-2-kinase/fructo-2,6-bisphosphatase); PFKFB, 6-phosphofructo-2-kinase/fructo-2,6-bisphosphatase isoform; PPP, pentose phosphate pathway; OCR, oxygen consumption rate; PI, phosphatidylinositol; FTICR-MS, Fourier transform ion cyclotron resonance-mass spectrometry.

cell, which may be useful for understanding disease mechanisms and developing targeted therapies. Optimizing the metabolism of cells prior to their transplantation could provide a new avenue to improve the effectiveness of cell therapy for patients with diabetes.

Experimental Procedures

Materials—Antibodies used for immunoblotting and flow cytometry are shown in supplemental Tables S1 and S2. DMEM/F12 containing L-glutamine, D-glucose, and pyruvic acid was purchased from US Biological (Swampscott, MA). EmbryoMax® ES cell qualified fetal bovine serum, EmbryoMax® ES cell qualified penicillin-streptomycin solution, and ESGRO® LIF were purchased from Millipore (Darmstadt, Germany). Recombinant human FGF basic was purchased from Peprotech (Rocky Hill, NJ). Recombinant epidermal growth factor was purchased from Sigma. Insulin-transferrin-selenium (500×) was purchased from Lonza (Walkersville, MD). Humulin R (used for insulin sensitivity experiments) was from Eli Lilly. All other reagents were from Sigma-Aldrich, unless indicated otherwise.

Cell Isolation and Culture—All animal procedures were performed in compliance with the National Institutes of Health Guide for the Care and Use of Laboratory Animals and were approved by the University of Louisville Institutional Animal Care and Use Committee. Murine CPCs were isolated from 2.5–3-month-old male B6.BKS(D)-*Lepr^{db}*/J (*db/db*) mice and C57BL/6J (WT) (The Jackson Laboratory, Bar Harbor, ME). After outgrowth, the CPCs were subjected to sequential sorting for c-kit$^+$/lin$^-$ markers using magnetic immunobeads (29, 30). As described previously (30, 31), the CPCs were cultured in growth medium. Passages 3–9 were used for these studies.

Proliferation, Viability, and Differentiation Measurements—Cell proliferation was assessed by counting cells using a hemocytometer or a BD Accuri C6 flow cytometer, as described previously (31). Cell viability was assessed by lactate dehydrogenase assay, as described previously (31). Differentiation of CPCs was assessed by quantitative RT-PCR after incubating cells in DMEM/F-12 medium containing 2% FBS, 1% penicillin/streptomycin, and 10 nM dexamethasone (32–34).

Gene Expression and Protein Abundance Analyses—Commitment to cardiovascular lineages was assessed by measuring cell type-specific gene expression by quantitative RT-PCR. For quantitative RT-PCR, mRNA was isolated from CPCs using TRIzol reagent (Invitrogen), and RNA quantity and purity were estimated by measuring absorbances at 260 and 280 nm using a Nanodrop spectrophotometer (Thermo Scientific). 2 μl of cDNA was used in a reaction mixture containing SYBR green (VWR, Radnor, PA) and oligo primers (Integrated DNA Technologies, Inc., Coralville, IA). Primers used for quantitative RT-PCR are shown in supplemental Table S3. For Western blotting, 0.5–50 μg of protein from crude CPC lysates were applied to each lane of a 12.5 or 10.5–14% Bis-Tris-HCl gel and electrophoresed. The separated proteins were then electroblotted onto a PVDF membrane, and immunoblotting was performed as described (31). Immunoreactive bands were detected using a Typhoon variable mode imager (GE Healthcare) or a Fuji LAS-3000 Bio Imaging analyzer after exposure to ECL detection reagent. Band intensities were quantified using TotalLab TL120 or ImageQuantTL software.

Extracellular Flux Analysis—Mitochondrial activity and surrogate measures of glycolytic flux were measured in WT and *db/db* CPCs, similar to that described previously (31, 35).

Mitochondrial Abundance Measurements—Mitochondrial abundance in CPCs was estimated by mitochondrial DNA abundance relative to nuclear DNA and by citrate synthase activity, as described by us previously (36). Primers for cytochrome *b* (mitochondrial DNA) and β-actin (nuclear DNA) were used; the sequences are cytochrome *b*, 5′-TTGGGTTGTTTGATCCTGTTTCG-3′ and 5′-CTTCGCTTTCCACTTCATCTTACC-3′; and β-actin, 5′-CAGGATGCCTCTCTTGCTCT-3′ and 5′-CGTCTTCCCCTCCATCGT-3′. Citrate synthase assay was performed in 100 mM Tris-HCl, pH 8.0, containing 1 mM EDTA, 1 mM 5′,5′-dithiobis 2-nitrobenzoic acid, and 10 mM acetyl-CoA. The reactions were initiated by addition of 10 mM oxaloacetate. Absorbance at 420 nm was measured for 10 min after the addition of protein from CPC lysates. Citrate synthase activity is expressed as μmol/min/mg protein.

Preparation of Replication-deficient PFK2 Adenovirus—Adenoviral vectors were made and purified by Vector Biolabs (Malvern, PA) using cDNA for a mutant form of rat liver 6-phosphofructo-2-kinase/Fru-2,6-P_2 bisphosphatase (*i.e.* the PFKFB1 isoform of PFK2). This bifunctional enzyme has been re-engineered by site-directed mutagenesis to have single-amino acid point mutations (S32A and H258A), which yield an enzyme having phosphofructo-2-kinase activity and no bisphosphatase activity (37–40). A 1.4-kb BamHI/NheI fragment of a pLenti6–3×FLAG-pd-PFK2 plasmid was subcloned into a CCM(+) shuttle vector, which has dual CMV promoters to drive expression of both GFP and the inserted gene. The backbone of the adenoviral vector is type 5 (dE1/E3). An Ad-GFP control virus was also purchased from Vector Biolabs.

Radiometric Determination of Glycolytic Flux—Glycolytic flux was determined by analyzing the conversion of [5-^{3}H]glucose to $[^3H]_2O$, as described previously (31). Briefly, CPCs were grown in 6-well plates to ~80% confluency. Reaction medium (DMEM/F-12 medium containing 1 mM L-glutamine, 5.5 mM D-glucose, and 2 μCi/ml [5-^{3}H]glucose (Moravek Biochemicals)) was added and incubated at 37 °C for 3 h. Then 50 μl of the reaction medium was pipetted into 1.5-ml microcentrifuge Eppendorf tubes containing 50 μl of 0.2 N HCl. The microcentrifuge tubes, with the tube tops removed, were placed in 20-ml scintillation vials containing 0.5 ml of distilled water. The vials were sealed and incubated for 48 h at room temperature to allow for evaporative diffusion of the $[^3H]_2O$ in the microfuge tubes into the scintillation vials. To account for incomplete equilibration of $[^3H]_2O$ and background, in parallel vials, known amounts (μCi) of [5-^{3}H]glucose and $[^3H]_2O$ (Moravek Biochemicals) were placed in microcentrifuge tubes, which were also placed into separate scintillation vials containing 0.5 ml of distilled water. Following the incubation, the microcentrifuge tubes were removed, and 10 ml of scintillation fluid was added to each vial. Radioactivity was then measured by scintillation counting. Glucose utilization was calculated using the formula reported by Ashcroft *et al.* (41), taking into account the

specific activity of the [5-^{3}H]glucose, incomplete equilibration, and background, the ratio of unlabeled and labeled glucose, and scintillation counter efficiency.

Stable Isotope Tracing—Isolated WT and *db/db* CPCs were incubated with 5 mM [$^{13}C_6$]glucose in 6-well plates for 3 or 18 h, quenched in cold acetonitrile, and extracted in acetonitrile: water:chloroform (v/v/v, 2:1.5:1), similar to that described previously (42–44), to obtain the polar, non-polar, and insoluble proteinaceous fractions. The non-polar (lipid) layer was collected, dried under a stream of nitrogen gas, and reconstituted in 0.1 ml of chloroform:methanol:BHT (2:1 + 1 mM) mixture. The extract was further diluted 10× with 1 mM BHT solution in methanol and used for Fourier transform ion cyclotron resonance-mass spectrometry (FTICR-MS) analysis.

For stable isotope nucleotide analysis, the samples were prepared using a previously published protocol (43), with slight modifications. Briefly, lyophilized polar extracts were reconstituted in 50 μl of 5 mM aqueous hexylamine (adjusted to pH 6.3 with acetic acid) (solvent A). Samples were then loaded onto a 100-μl capacity C18 tip (Pierce-Thermo Fisher Scientific) followed by washing twice with 50 μl of solvent A. The metabolites were eluted with 70% solvent A and 30% 1 mM ammonium acetate in 90% methanol, pH 8.5 (solvent B). The resulting eluates were diluted 3× with methanol and analyzed via FTICR-MS.

FTICR-MS Analysis—Lipid and nucleotide spectra were acquired using a hybrid linear ion trap-FT-ICR mass spectrometer (Finnigan LTQ FT; Thermo Electron, Bremen, Germany), equipped with a TriVersa NanoMate ion source (Advion BioSciences, Ithaca, NY) with an A electrospray chip (nozzle inner diameter, 5.5 μm). The TriVersa NanoMate was operated by applying 1.5 kV with 0.5 psi head pressure in positive ion mode and 1.6 kV and 0.7 psi in the negative mode. High mass accuracy data were collected using the FT-ICR analyzer over a mass range from 150 to 1600 Da (lipids; + and − mode) and 150–850 Da (nucleotides; − mode) for 15 min at the target mass resolution of 400,000 at 400 m/z. The LTQ-FT was tuned and calibrated according to the manufacturer's default standard recommendations, to achieve mass accuracy of 2 ppm or less.

Stable Isotope Data Analysis—The FT-ICR MS spectra were exported as exact mass lists into a spreadsheet file using QualBrowser 2.0 (Thermo Electron). Assignments of all isotopologue peaks of metabolites were performed based on their accurate mass matching (m/z window ± 3 ppm), and natural isotope abundance contributions from each of the isotopologues in the MS data were stripped using MetSign.

Coupling quotients were calculated using fractional enrichment values of isotopologues. For this, we calculated quotients of isotopologue fractional enrichment values of two independent pathways (*e.g.* the $m + 5$ isotopologue of UTP synthesized via the pentose phosphate pathway and the [$^{13}C_3$]glycerol isotopologue of phosphatidylinositol synthesized via the glycerolipid pathway), which provides an index of relative metabolic pathway coupling.

Statistical Analysis—The data are presented as means ± S.E. Multiple groups were compared using one-way or two-way analysis of variance, followed by Tukey or Sidak post-tests. Unpaired Student's t test was used for two-group comparisons. A p value ≤ 0.05 was considered significant.

Results

Diabetic CPCs Show Persistent Defects in Competency—We first compared the general phenotype of WT and *db/db* CPCs. Similar to WT CPCs, *db/db* cells had a largely spindle-like morphology (Fig. 1*A*). As reported previously, the cells retained only ~5–10% positivity for c-kit after sorting and culture (30, 31), and both nondiabetic and diabetic cells were >90% positive for the mesenchymal cell marker CD29 and Sca1 and <5% positive for CD45 (Fig. 1, *B* and *D*). Both nondiabetic and diabetic cells showed relatively low surface expression of CD73, showed relatively high expression of 105, and were largely negative for CD31 and CD34 (Fig. 1*D*); both the WT and the *db/db* cells were <0.1% positive for SSEA1, SSEA3, and SSEA4. There were striking differences, however, in the expression of CD90 in diabetic cells. Diabetic CPCs showed nearly 80% positivity for CD90 compared with only ~6% positivity in nondiabetic cells (Fig. 1, *C* and *D*).

We next examined common measures of cell competency. Diabetic cells demonstrated lower rates of proliferation (Fig. 2, *A* and *B*), as well as a decreased ability to withstand hydrogen peroxide stress (Fig. 2*C*). Of note, in WT cells, the addition of exogenous leptin had no effect on proliferative capacity of CPCs (data not shown), suggesting that defective leptin signaling is unlikely to contribute to the loss of competence in diabetic CPCs.

Although it is unlikely that differentiation of CPCs contributes directly to myocardial regeneration, differentiation of stem cells has been suggested to reflect their capacity to invoke reparative responses in injured tissue (22, 45). Therefore, we next examined gene programs that might indirectly regulate their restitutive actions during cell therapy. Compared with WT CPCs, diabetic CPCs demonstrated lower expression of markers of cardiac (*Tnnt2*), endothelial (*Flk1*), and smooth muscle (*Acta2*) lineages upon exposure to differentiation conditions (Fig. 2*D*). Although fibroblastic program markers (*Col1a1*, *Col3a1*, and *Tgfb1*) were not different between WT and *db/db* CPCs, genes of the core preadipocyte gene program, *i.e. Cyp7b1* and *Bhlhe22* (46), were remarkably higher in diabetic CPCs. In addition, *Lox*, which regulates cell commitment to an adipocyte lineage (47–49) was elevated upon differentiation only in diabetic cells (Fig. 2*D*). Collectively, these results indicate that diabetes causes persistent losses in proliferation and survival and disrupts the differentiation profile of CPCs.

Diabetic CPCs Are Insulin-resistant—Defective Akt signaling is a characteristic feature of insulin resistance in diabetic cells and tissues (50). To determine whether diabetes also causes changes in insulin signaling in CPCs, we examined Akt signaling after treatment with insulin. Insulin promoted concentration-dependent increases in Akt phosphorylation that became largely apparent at concentrations ≥10 nM (Fig. 3*A*). Treatment of cells with palmitic acid, which is known to lead to insulin resistance (51), diminished insulin-induced Akt phosphorylation (Fig. 3*B*), suggesting that dyslipidemia could contribute to insulin resistance in CPCs.

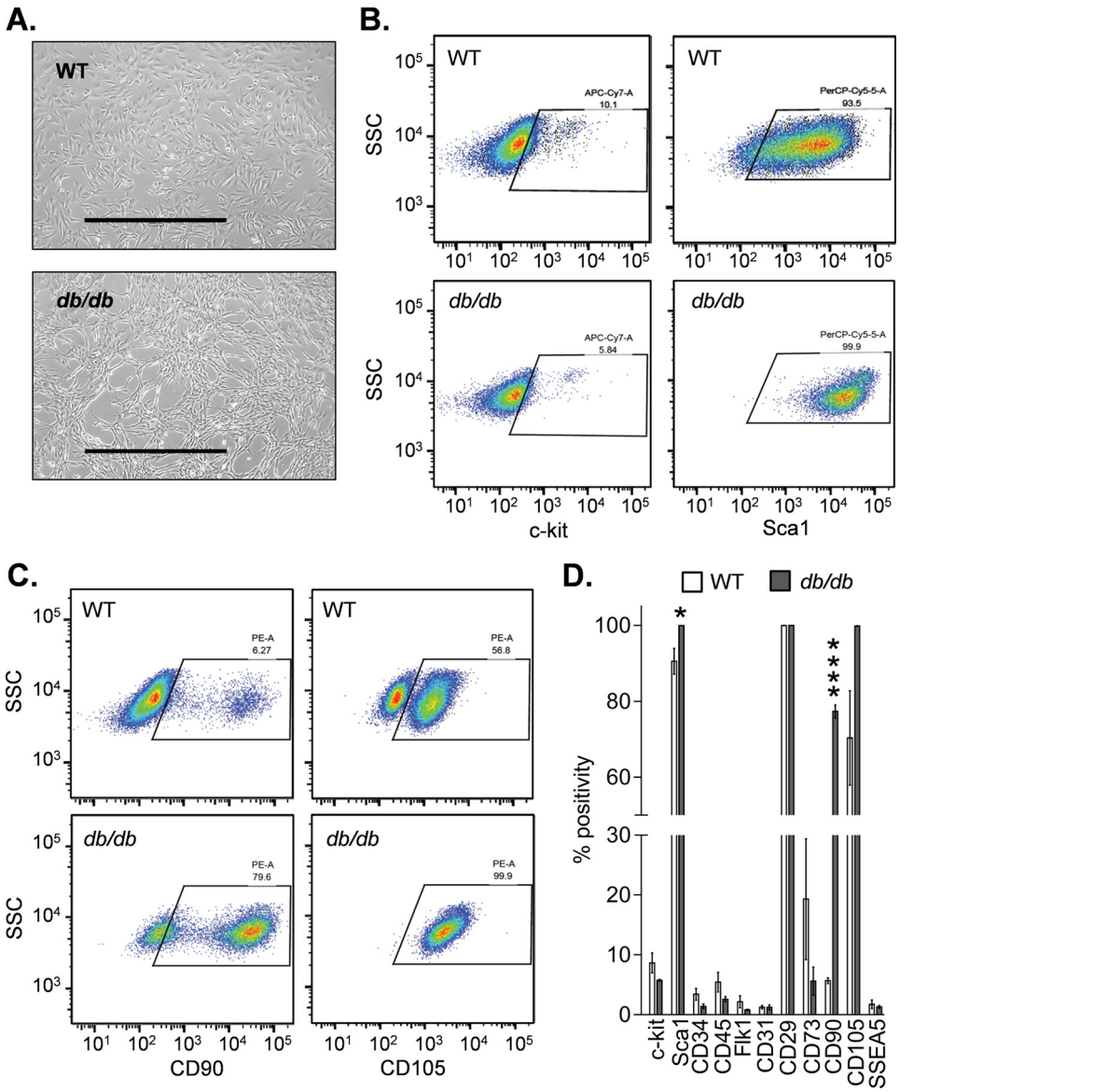

FIGURE 1. **Diabetic and nondiabetic CPCs display features characteristic of mesenchymal cells.** Gross morphology and surface marker expression in CPCs isolated from nondiabetic (WT) and diabetic (*db/db*) mice are shown. *A*, brightfield images of WT and *db/db* CPCs. *Scale bars*, 1000 μm. *B*, representative flow cytometric dot plots of c-kit and Sca1. *C*, flow cytometric dot plots of CD90 and CD105. *D*, summary of surface marker expression. The data are representative of three independent experiments. *, $p \leq 0.05$; ****, $p < 0.0001$ *versus* corresponding surface marker in the WT group.

To determine whether diabetes causes long lasting changes in insulin signaling, we examined Akt signaling and insulin receptor phosphorylation in WT- and *db/db*-derived CPCs. As shown in Fig. 3*C*, diabetic CPCs showed significantly higher basal Akt phosphorylation compared with WT CPCs, yet they were incapable of significantly inducing Akt phosphorylation further upon treatment with insulin. Interestingly, the basal level of Akt phosphorylation in *db/db* CPCs was accompanied by higher basal phosphorylation of tyrosine residues (Tyr^{1158}, Tyr^{1162}, and Tyr^{1163}) of the insulin receptor, indicating upstream deregulation of insulin signaling (Fig. 3*D*). Collectively, these results indicate that diabetes diminishes insulin responsiveness in CPCs yet causes persistent activation of the insulin signaling cascade.

Diabetic CPCs Show Persistent Dysregulation of Glucose Metabolism—To determine whether insulin resistance in diabetic CPCs is associated with changes in intermediary metabolism, we examined both mitochondrial and glycolytic metabolism in WT and *db/db* CPCs. Mitochondrial consumption of oxygen was lower in *db/db* CPCs (Fig. 4*A*), whereas basal extracellular acidification was modestly increased (Fig. 4*B*), leading to a marked decrease in the basal oxygen consumption rate (OCR)/extracellular acidification rate (ECAR) ratio (Fig. 4*C*), an index of cellular reliance on mitochondrial *versus* glycolytic metabolism. In *db/db* cells, the generally lower OCR levels and the lower carbonyl cyanide *p*-trifluoromethoxyphenylhydrazone-stimulated ECAR levels (which commonly derive from protons linked with respiratory CO_2 production (52)) could suggest lower abundance of mitochondria. To test this, we measured three markers of mitochondrial content: the abundance of several key respiratory complex subunits under undifferentiated and differentiated conditions; citrate synthase activity; and relative mitochondrial DNA content. Although differentiation in dexamethasone-containing medium promoted up-reg-

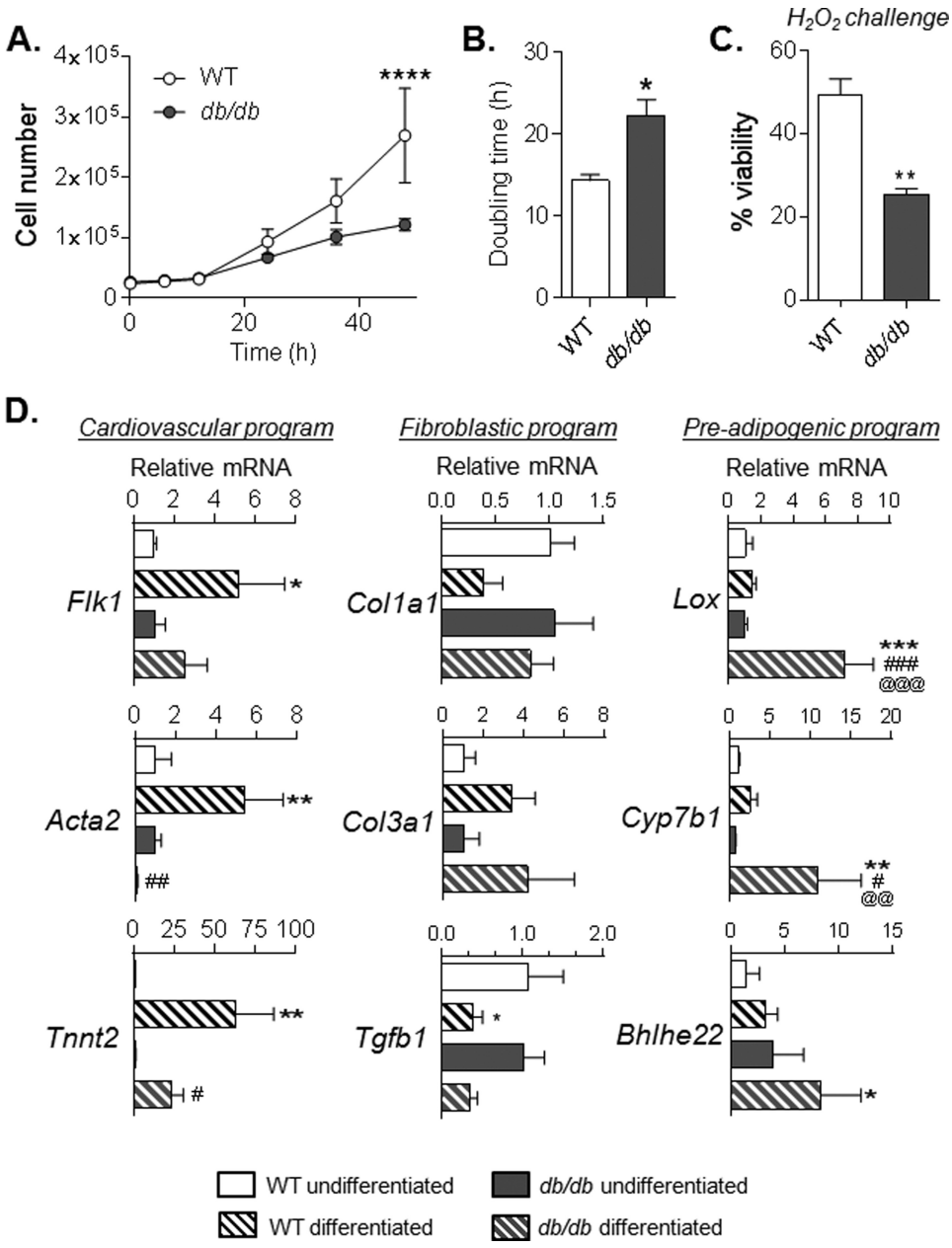

FIGURE 2. **Diabetes causes sustained impairment in factors of competency in culture.** Measures of competence in CPCs isolated from WT and *db/db* mice are shown. *A*, traces of cell proliferation over a 48-h period. *B*, cell doubling time, calculated from data in *A*. *C*, cell survival, measured by lactate dehydrogenase assay, after a 16-h challenge with 500 μM H_2O_2. *, $p \leq 0.05$; **, $p \leq 0.01$ *versus* WT cells. *D*, relative expression of transcripts indicative of cardiovascular, fibroblastic, and preadipogenic gene programs. Each plot represents three independent experiments. *, $p \leq 0.05$; **, $p \leq 0.01$ *versus* WT undifferentiated. #, $p \leq 0.05$; ##, $p \leq 0.01$; ###, $p \leq 0.001$ *versus db/db* undifferentiated. @@, $p \leq 0.01$; @@@, $p \leq 0.001$ *versus* WT differentiated.

ulation of several respiratory subunits (*e.g.* ATP synthase subunit α, cytochrome *c* oxidase subunit 1, and succinate dehydrogenase subunit B), there were no differences in subunit abundance between WT and *db/db* CPCs (Fig. 4*D*). Interestingly, the diabetic CPCs showed ~30% higher citrate synthase activity levels compared with WT cells (Fig. 4*E*); however, mitochondrial DNA content was not different between nondiabetic and diabetic CPCs (Fig. 4*F*). Collectively, these results suggest that the deficit in mitochondrial activity in diabetic CPCs is not due to a lower abundance of mitochondria.

To determine whether increased reliance on glycolytic activity in diabetic CPCs may be due to remodeling of glucose metabolism, we next measured the abundances of several key proteins in glucose metabolism and glycolysis by immunoblotting. Although levels of glucose transporter 1, hexokinase 1 and 2, phosphofructokinase-bisphosphatase (PFKFB) 2, GAPDH, pyruvate kinase M 1/2, and lactate dehydrogenase A were not significantly different, the relative levels of glucose transporter 4 and PFKFB3 were higher in diabetic cells (Fig. 4, *G–I*). Collectively, these data indicate that diabetes persistently increases glycolysis in CPCs, which may be related to an increase in PFKFB3.

Diabetes Causes Uncoupling of Biosynthetic Pathways in CPCs—The up-regulation of PFKFB3 in diabetic CPCs would suggest an increase in PFK1 activity, the rate-limiting enzyme and committed step in glycolysis (53, 54). Because increased

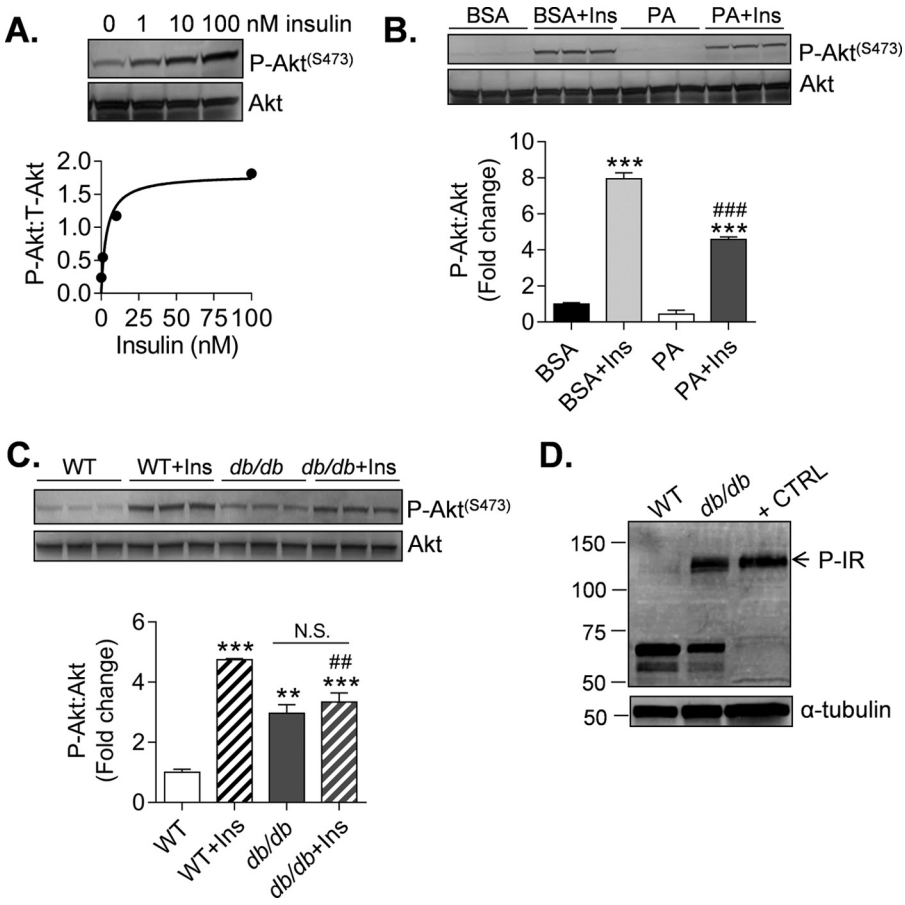

FIGURE 3. **Diabetes causes insulin resistance in CPCs.** Immunoblots of markers of insulin resistance in CPCs are shown. *A*, phosphorylation of Akt (Ser[473]) from lysates derived from WT CPCs treated with 0–100 nM insulin for 15 min. The data are shown as discrete points. The *curve* is a best fit of the hyperbolic equation $y = (\max \times x)/(K_{1/2} + x)$ to the data. Best fit values of max and $K_{1/2}$ are 1.80 AU and 3.62 nM ($r^2 = 0.93$). *B*, P-Akt measurements from lysates derived from WT CPCs treated with 100 μM palmitate (*PA*) conjugated to BSA or BSA alone (vehicle) for 3 h. The cells were then exposed to 10 nM insulin (*Ins*) for 15 min prior to harvest. The results represent three technical replicates/group. **, $p \leq 0.01$; ***, $p \leq 0.001$ *versus* corresponding group not treated with insulin. ###, $p \leq 0.01$ *versus* BSA + Ins. *C*, P-Akt measurements from lysates derived from WT and *db/db* CPCs treated without or with 10 nM insulin for 15 min. The results represent three technical replicates/group. **, $p \leq 0.01$; ***, $p \leq 0.001$ *versus* WT; ##, $p \leq 0.01$ *versus* WT + Ins. *D*, basal insulin receptor phosphorylation (*P-IR*) in WT and *db/db* CPCs. HUVECs stimulated with insulin were used as a positive control (+ *CTRL*).

activity at this critical step in glycolysis might affect ancillary pathways of glucose metabolism (*e.g.* Refs. 55–57), we next examined relative glucose carbon flux through an "upstream" biosynthetic pathway controlling nucleotide biosynthesis and redox state (the pentose phosphate pathway (PPP)) and a "downstream" pathway involved in esterified lipid biosynthesis (the glycerolipid pathway (GLP)) (Fig. 5). For this, the CPCs were incubated with universally labeled (U) [^{13}C]glucose for 3 or 18 h, and entry of glucose-derived ^{13}C into end products of the PPP and the GLP was examined by stable isotope-resolved metabolomics (Fig. 6, *A* and *D*) (42–44, 58). Incorporation of ^{13}C into the ribose ($m + 5$ isotopologue) moiety of the purine ATP was lower in *db/db* CPCs after 3 h of incubation with U-[^{13}C]glucose (Fig. 6*C*, *inset*), and after 18 h, there remained significantly lower incorporation of ^{13}C carbon in the $m + 6$ and $m + 7$ isotopologues, which correspond to the adenine nucleoside portion of the molecule (Fig. 6, *B* and *C*). Similar results were observed for the purine nucleotide GTP (data not shown). Although ^{13}C incorporation into the pyrimidine UTP appeared similar between WT and *db/db* cells after 3 h of incubation with U-[^{13}C]glucose, by 18 h, WT CPCs showed markedly higher incorporation of ^{13}C into the ribose ($m + 5$) moiety compared with *db/db* CPCs. Moreover, the unlabeled pool of UTP was significantly higher in the diabetic CPCs (Fig. 6, *E* and *F*). Taken together, these data indicate that type 2 diabetes decreases PPP flux in CPCs.

Next, we assessed the GLP, a pathway that uses 3-carbon products of glycolysis (*i.e.* dihydroxyacetone phosphate) to synthesize glycerol; glycerol provides the backbone for esterification of fatty acids into phospholipids (Fig. 7*A*). Although there was no significant accumulation of ^{13}C from U-[^{13}C]glucose into the glycerol ($m + 3$) moiety of PI within 3 h (Fig. 7*E*), after 18 h of incubation, there was a ~50% increase in the ^{13}C-labeled glycerol portion of PI, and a corresponding decrease in the unlabeled PI pool (Fig. 7, *C*, *D*, and *F*). Diabetes did not affect ^{13}C incorporation into fatty acids of PI or the levels of metabolites having ^{13}C in both the glycerol moiety and fatty acids. Collectively, these data indicate lower glucose-derived carbon flux through the PPP and relatively higher flux in the GLP.

To estimate and compare metabolic pathway coupling in WT and diabetic CPCs, we calculated coupling quotients using isotopologue fractional enrichment values of metabolites synthesized by each ancillary pathway (Table 1). Here, the ^{13}C frac-

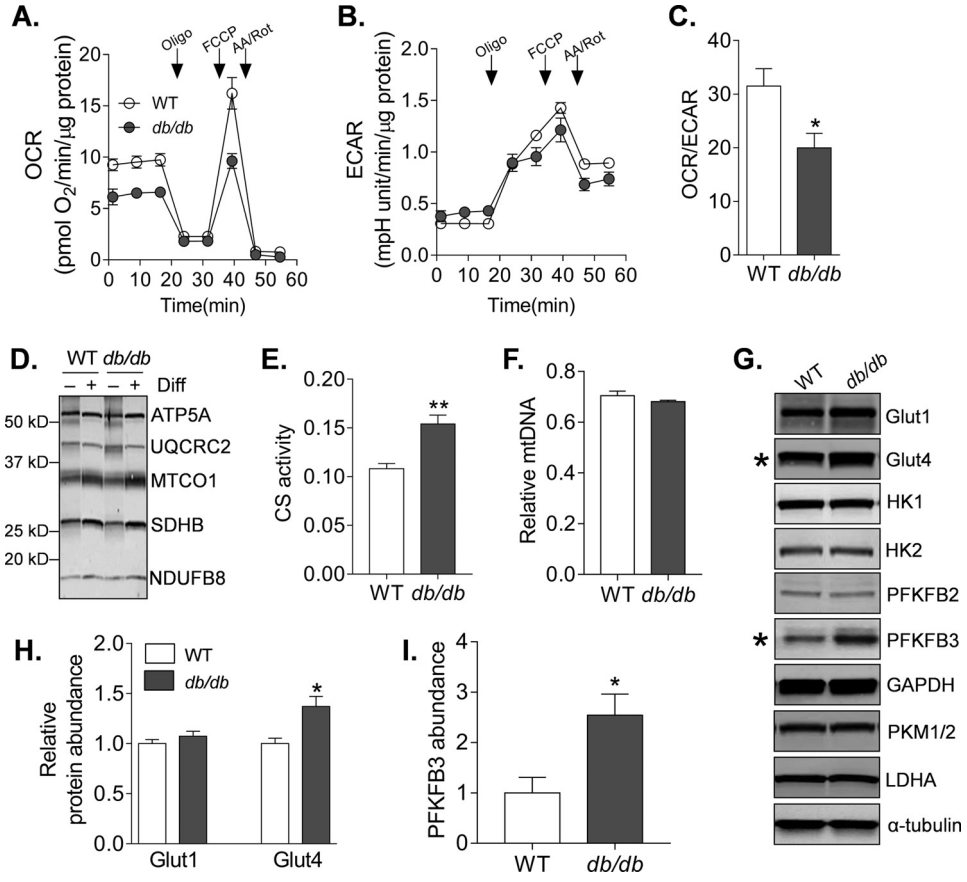

FIGURE 4. **Diabetes deranges intermediary metabolism in CPCs.** Indices of mitochondrial and glycolytic metabolism in nondiabetic and diabetic CPCs are shown. *A*, representative OCR trace of WT and *db/db* CPCs. After three baseline OCR recordings, the CPCs were exposed sequentially to oligomycin (*Oligo*), carbonyl cyanide *p*-trifluoromethoxyphenylhydrazone (*FCCP*), and a mixture of antimycin A and rotenone (*AA/Rot*), with OCR measurements recorded after addition of each compound. *B*, representative trace of the ECAR in the CPCs. *C*, OCR/ECAR ratio in WT and *db/db* CPCs. The plot represents four independent experiments. *D*, representative Western blot of respiratory subunit complexes in WT and *db/db* CPCs cultured in growth medium or differentiation (*Diff*) medium. *E*, citrate synthase activity in WT and *db/db* CPCs. Plot represents three independent experiments. *F*, relative mitochondrial DNA content in WT and *db/db* CPCs. Plot represents three independent experiments. *G*, representative Western blots of glucose metabolism enzymes, particularly those important to glycolysis. The plots are representative of at least three replicates/group. *H*, quantification of glucose transporters 1 (*Glut1*) and 4 (*Glut4*) immunoblots derived from experiments indicated in *G*. The plots represent three replicates/group. *I*, quantification of PFKFB3 derived from experiments indicated in *E*. The plot represents three independent experiments. *, $p \leq 0.05$; **, $p \leq 0.01$ *versus* WT CPCs.

tional enrichment values of isotopologues of purine and pyrimidine nucleotides (*e.g.* ribose; $m + 5$ isotopologue) and glycerophospholipids (glycerol) were used to calculate coupling quotients, relating the PPP and GLP. Together, the stable isotope tracing profile and coupling quotients appear to localize the defect to steps relating the "preparatory" and "payoff" phases of glycolysis, which is consistent with our other glucose metabolism flux measurements, as well as our immunoblotting data. Collectively, these results suggest that diabetes-induced up-regulation of PFKFB3 increases glycolytic activity at the PFK step of glycolysis, which uncouples ancillary biosynthetic pathways of glucose metabolism.

Increasing Glycolysis Is Sufficient to Decrease Mitochondrial Activity and Diminish Proliferation—PFKFB3 is an isoform of PFK2 known to increase the glycolytic rate by promoting activation of PFK1 (Refs. 59–64 and Fig. 5). Interestingly, in addition to increasing glycolysis, PFKFB3 is capable of migrating to the nucleus where it can regulate proliferation (65); other isoforms of PFKFB do not demonstrate nuclear localization. Therefore, to determine specifically how activation of glycolysis at the PFK step regulates CPC function, we expressed a mutated form of PFKFB1 (phosphatase-deficient PFK2; pd-PFK2) that has no bisphosphatase activity (37–40). Like PFKFB3, the pd-PFK2 enzyme has only phosphofructo-2-kinase activity, which increases intracellular levels of fructose-2,6-bisphosphate to activate PFK1. This mutant enzyme has been shown to increase glycolysis *in vitro* and *in vivo* in multiple cell types including cardiac myocytes (40) and liver (39, 66). The bicistronic vector also contained GFP, which was used to determine relative transduction efficiency (typically >75%) in CPCs (Fig. 8*A*). As shown in Fig. 8*B*, transduction of the cells with the mutant PFK2 enzyme led to marked expression of the protein, which was absent in non-transduced control and Ad-GFP-transduced cells. As expected, transduction of CPCs with pd-PFK2 increased the glycolytic rate, as shown by increased ECAR values (Fig. 8*C*) and higher radiometric values of glycolytic flux (Fig. 8*D*). Consistent with our previous study showing a glucose concentration-dependent diminution of mitochondrial activity in CPCs (31), high rates of glycolysis caused by expression of pd-PFK2 decreased oxygen consumption by ~50% upon addition of glucose to the medium (Fig. 8*E*). In addition, high rates of glycolysis caused by pd-PFK2 expression were sufficient to

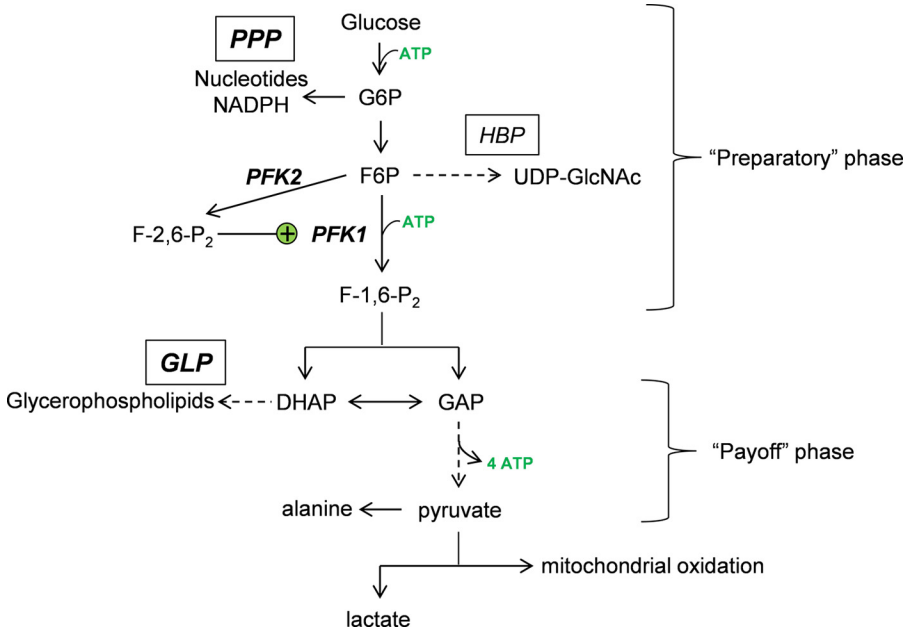

FIGURE 5. **Schematic of glycolysis and ancillary glucose metabolism pathways.** Once glucose enters the cell, it can be phosphorylated to form glucose-6-phosphate (*G6P*), which isomerizes to fructose-6-phosphate (F6P). The F6P is then phosphorylated by PFK1—the major rate-limiting and committed step in glycolysis—to fructose-1,6-bisphosphate (*F-1,6-P*$_2$). These reactions comprise the preparatory phase of glycolysis and utilize ATP. In addition, glycolytic metabolites in this phase of glycolysis serve as precursors to several ancillary biosynthetic pathways, including the PPP and the hexosamine biosynthetic pathway (*HBP*), as well as the polyol pathway (not shown) and glycogen synthetic pathway (not shown). The payoff phase commences with the splitting of fructose-1,6-bisphosphate into DHAP and GAP. DHAP is a precursor for the GLP, important for the synthesis of glycerophospholipids, and it can be isomerized to GAP. GAP is oxidized and phosphorylated to 1,3-bisphosphoglycerate. Energy (ATP) is released as these 1,3-bisphosphoglycerate molecules are converted to pyruvate, which is then transaminated to alanine, converted to lactate, or oxidized in mitochondria. The activity of PFK1, which sits at the nexus between the preparatory and payoff phases, is increased by the product of 6-phosphofructo-2-kinase (PFK2), fructose-2,6 bisphosphate (*F-2,6-P*$_2$).

diminish CPC proliferation (Fig. 8*F*). Collectively, these data suggest that elevation of glycolysis in diabetic CPCs is likely due to an increase in the expression of PFKFB3 and that activation of PFK in normal CPCs at least partially phenocopies diabetes-induced impairment of CPCs.

Discussion

In this study, we describe a mechanism by which diabetes causes metabolic dysfunction in cardiac progenitor cells. We find that diabetes causes persistent changes in glucose metabolism in CPCs and that high reliance on glycolysis is associated with poor CPC competence. Convergent evidence derived from immunoblotting, isotope tracing, and extracellular flux measurements indicates that diabetes up-regulates PFKFB3, the product of which activates the rate-limiting and committed step of glycolysis, F6P → fructose-1,6-bisphosphate. This step is best positioned to coordinate and partition glucose-derived carbons into biosynthetic pathways in the cell and could therefore contribute to diabetes-induced cell dysfunction. We find also that diabetes constitutively activates the insulin signaling pathway and diminishes mitochondrial activity. The increasing glycolytic rate at the PFK step in nondiabetic cells leads to losses in cell proliferation and mitochondrial activity redolent of diabetic CPCs. Additionally, these studies led to the development of a novel and simple approach, based on stable isotope tracing, to quantify the relationships between individual pathways of intermediary metabolism and to estimate their degree of uncoupling in disease. We propose that uncoupling of ancillary pathways of glucose metabolism is a primary cause of CPC dysfunction in diabetes.

Our findings are consistent with previous studies in the field and deepen our understanding of how diabetes impairs cell therapy-mediated myocardial repair. Two specific mechanisms have been implicated in diminution of CPC repair capacity in diabetes. Cells from type 1 diabetic models were shown to cause mitochondrial-engendered oxidative stress in CPCs (18), whereas type 2 diabetes was demonstrated to increase advanced glycation end product generation (19). A heightened rate of glycolysis could, in principle, be upstream of both mechanisms. Because extracellular glucose concentration contributes to glycolytic rate in CPCs (31), hyperglycemia would not only increase glycolytic flux but it could also elevate mitochondrial reactive oxygen species, as well as glyceraldehyde-3-phosphate (GAP), which is known to be a precursor for the advanced glycation end product, methyglyoxal (67). An increase in PFKFB3, leading to heightened glycolytic rates, would also be expected to increase the formation of GAP and elevate endogenous levels of reactive species. Additionally, the increase in PFKFB3 appears to be sufficient to lower mitochondrial activity in diabetic cells. Our previous studies show that exposure to glucose decreases mitochondrial activity in CPCs (31), which can be explained by the Crabtree effect (68, 69). Here, we demonstrate that increasing glycolytic rate in CPCs by expressing pd-PFK2 is sufficient to decrease mitochondrial activity and phenocopy the effects of diabetes on proliferation.

Our study also shows that CPCs isolated from the diabetic heart have a higher percentage of cells positive for CD90. This finding is consistent with human studies showing that the abundance of CD90$^+$ cells is increased in cardiosphere-derived

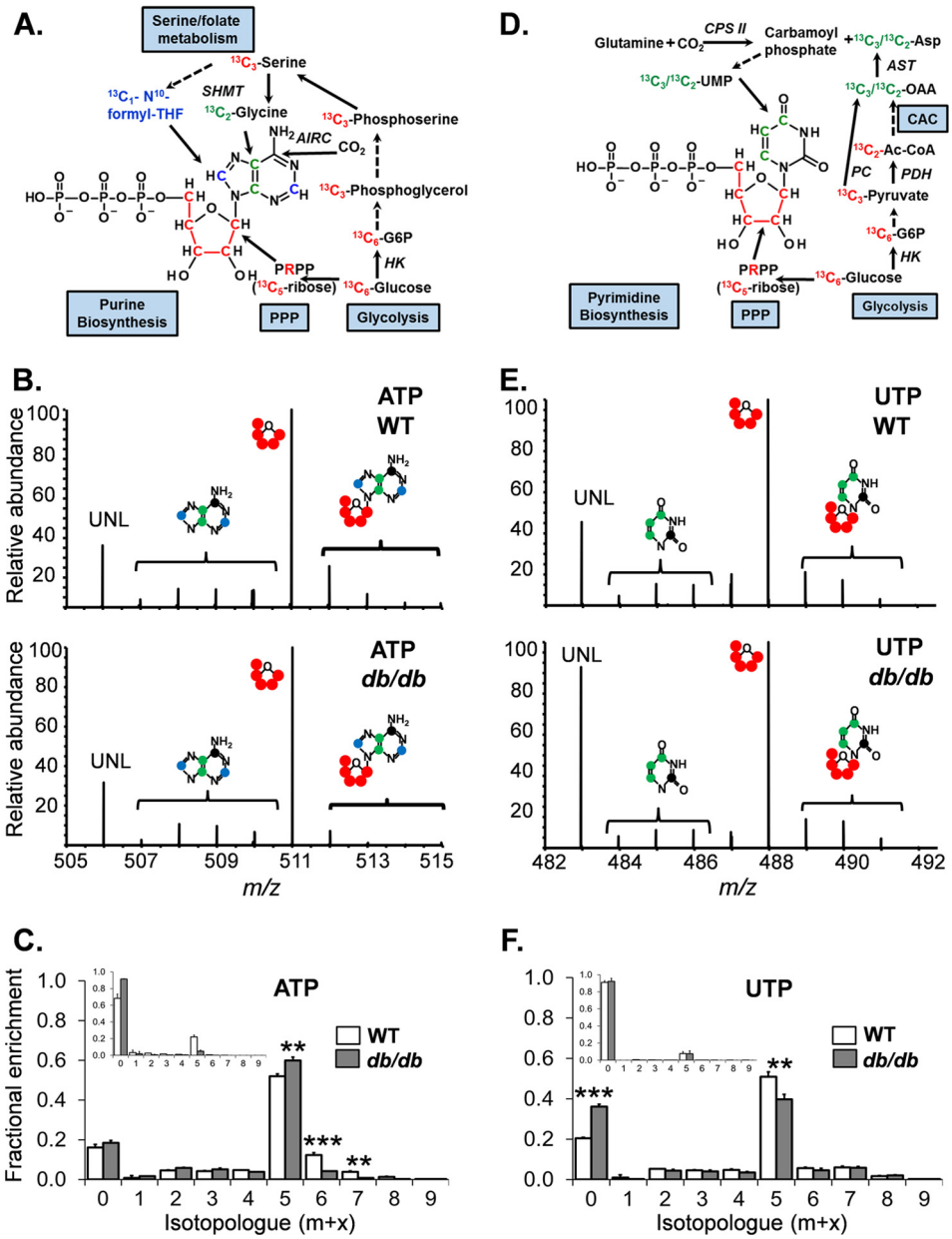

FIGURE 6. **Glucose-derived carbon incorporation into nucleotides is diminished in diabetic CPCs.** Stable isotope tracing of nucleotides in CPCs incubated with medium containing U-[^{13}C]glucose is shown. *A*, atom-resolved map illustrating the biological and biochemical history of ^{13}C incorporation into the purine ATP. *B*, representative FT-ICR mass spectra of ATP extracted from WT (*upper panel*) and *db/db* (*lower panel*) CPCs incubated with [^{13}C]glucose for 18 h. *C*, fractional enrichment values of ^{13}C in ATP after 18 h of incubation with U-[^{13}C]glucose. The *graph* represents triplicate values. *Inset*, fractional enrichment values of ^{13}C in ATP after 3 h of incubation with U-[^{13}C]glucose. The *inset* represents two replicates/group. *D*, atom-resolved map illustrating the biological and biochemical history of ^{13}C incorporation into the pyrimidine UTP. *E*, FT-ICR mass spectra of UTP extracted from WT (*upper panel*) and *db/db* (*lower panel*) CPCs incubated with U-[^{13}C]glucose for 18 h. *F*, fractional enrichment values of ^{13}C in UTP after 18 h of incubation with U-[^{13}C]glucose. The graph represents three replicates/group. *Inset*, fractional enrichment values of ^{13}C in UTP after 3 h of incubation with U-[^{13}C]glucose. The *inset* represents two replicates/group. **, $p \leq 0.01$; ***, $p \leq 0.001$ in corresponding isotopologue fractional enrichment in WT *versus db/db* cells.

cells isolated from diabetic patients (70), and it is important because CD90 positivity is associated with lower therapeutic efficacy in myocardial cell therapy (70, 71). It remains unclear how diabetes increases CD90 positivity in the CPC population or whether its expression contributes to altered metabolic pathways in hyperglycemic conditions.

We speculate that up-regulation of PFKFB3 may be an attempt by the cell to utilize excess glucose under hyperglycemic conditions; however, it is unclear why levels of the enzyme remain high in CPCs after isolation from the diabetic heart. Interestingly, PFKFB3 is highly expressed in adipocytes (72, 73) and cancer cells (54, 74), and it is up-regulated in diabetic liver (60). The enzyme generates fructose-2,6 bisphosphate (F-2,6-P_2), the actions of which override inhibition of PFK1 by inhibitors such as ATP, citrate, and phosphoenolpyruvate (59–64). This promotes feed-forward stimulation of glycolysis that is dependent primarily on glucose availability and uptake, which are not limiting in CPCs because they express considerable levels of glucose transporter 1 (Ref. 31 and Fig. 4). Interestingly, PFKFB3 was recently suggested to participate in a positive feed-

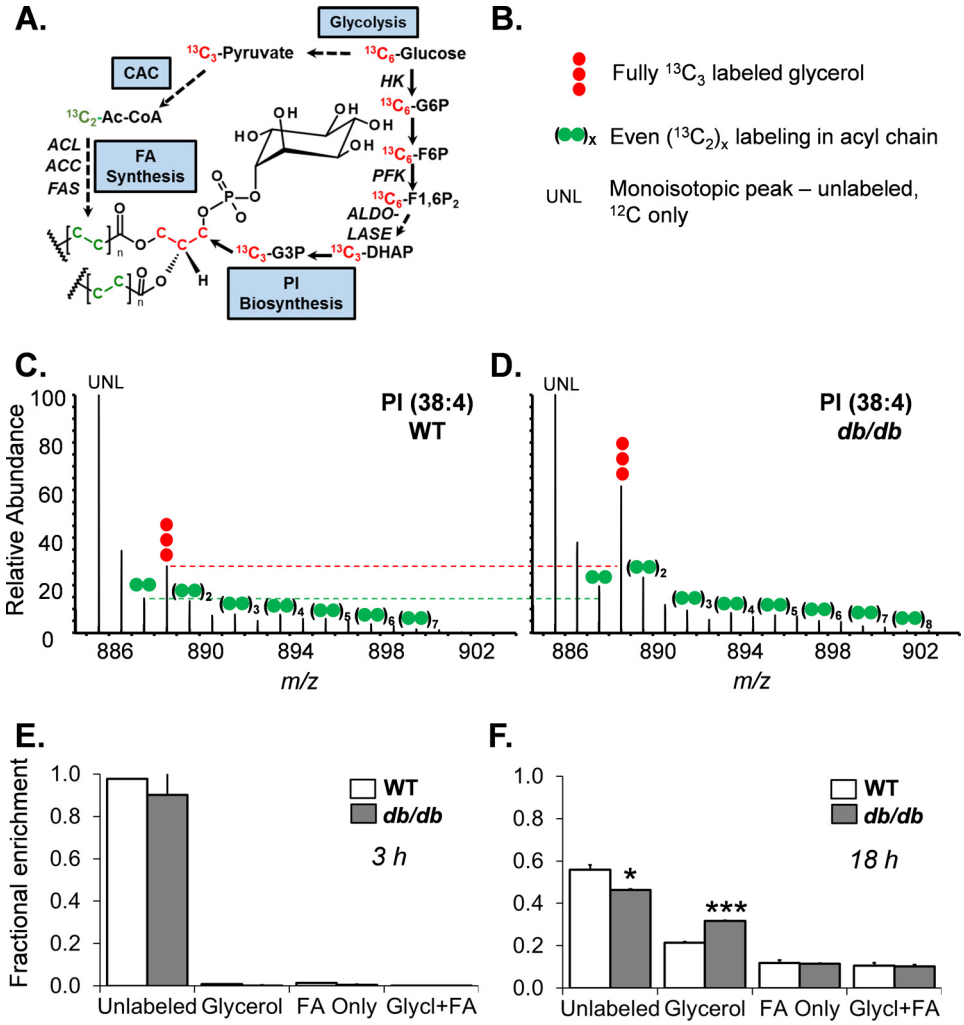

FIGURE 7. **Diabetes increases glycerolipid pathway flux in CPCs.** Stable isotope tracing of PI in CPCs incubated with medium containing U-[^{13}C]glucose is shown. *A*, atom-resolved map illustrating the biological and biochemical history of ^{13}C incorporation into the glycerolipid, PI. *B*, legend for mass spectral data in *C* and *D*. *UNL*, unlabeled. *C*, representative FT-ICR mass spectrum of PI extracted from WT cells after 18 h of culture in medium containing U-[^{13}C]glucose. *D*, representative FT-ICR mass spectrum of PI extracted from *db/db* CPCs after 18 h of culture in medium containing U-[^{13}C]glucose. *E*, fractional enrichment values of ^{13}C in PI after 3 h of incubation with U-[^{13}C]glucose. The plot represents two replicates/group. *F*, fractional enrichment values of ^{13}C in PI after 18 h of incubation with U-[^{13}C]glucose. The data represent three replicates/group. *, $p \leq 0.05$; ***, $p \leq 0.001$ in corresponding isotopologue fractional enrichment in WT *versus db/db* cells.

TABLE 1

Coupling quotients derived from stable isotope fractional enrichment data

CPCs derived from WT or db/db CPCs were cultured in growth medium containing [U-^{13}C]glucose. After 18 h, the cells were collected, and the polar and nonpolar fractions were assessed for ^{13}C incorporation in nucleotides and lipids, respectively. A relative coupling quotient between the PPP and the GLP was calculated by dividing the fractional enrichment values of the $m + 5$ ^{13}C isotopologue in the purines ATP and GTP and the pyrimidine UTP by the $m + 3$ isotopologue of glycerol in phosphatidylinositol (PI). The data represent three replicate samples/group.

Pathway couple	Metabolite couple	WT	*db/db*
PPP:GLP	ATP (5):PI (glycerol)	4.82 ± 0.13	3.04 ± 0.25[a]
	GTP (5):PI (glycerol)	4.25 ± 0.05	2.80 ± 0.13[a]
	UTP (5):PI (glycerol)	4.71 ± 0.10	2.00 ± 0.07[b]

[a] $p \leq 0.01$ *versus* WT CPCs.
[b] $p \leq 0.001$ *versus* WT CPCs.

back loop that causes hyperphosphorylation of Akt and increases glucose transporter 4 translocation (75). We show that Akt is hyperphosphorylated and that glucose transporter 4 abundance is elevated in diabetic CPCs, which may be caused by PFKFB3 or elevated glycolytic rates in general.

The question of how glycolysis regulates Akt and the insulin signaling pathway in CPCs is deserving of further study. The fact that both Ser^{473} of Akt and the Tyr^{1158}, Tyr^{1162}, and Tyr^{1163} residues of the insulin receptor (76) showed higher phosphorylation suggests that the entire IR/PI3K/Akt pathway is persistently activated in diabetic CPCs. One possibility is that metabolites of glycolysis promote Akt phosphorylation. Lactate, for example, has been shown to increase Akt by stimulating HIF1α expression (77) or by activating receptors receptor tyrosine kinases such as VEGFR2 (78), and it also activates G protein-coupled receptor 81 (79). Furthermore, it is possible that partitioning of glucose toward lactate (or ancillary biosynthetic pathways) could prevent it from being oxidized in mitochondria, thereby changing cellular redox signaling (80). The levels of other metabolites such as acetyl CoA (81) and UDP-GlcNAc (82) could also influence the activity of Akt, and both of these are expected to be affected by altered glycolytic rates.

Metabolites synthesized through pathways ancillary to glycolysis are essential for energy provision, as well as the biosyn-

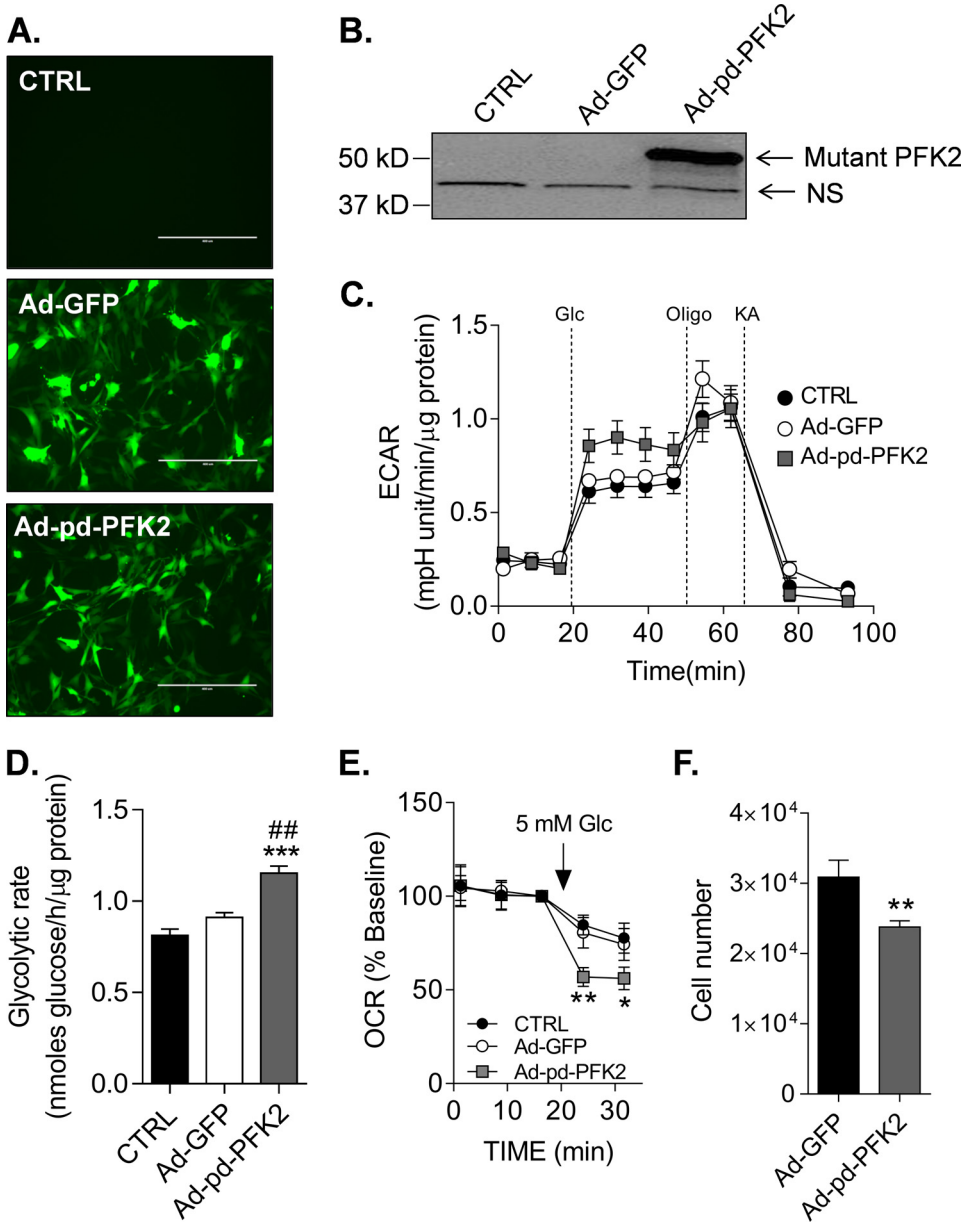

FIGURE 8. **Expression of a fructose-2,6-bisphosphatase-deficient PFK2 mutant phenocopies diabetes-induced losses of mitochondrial activity and proliferative capacity.** Effects of mutant PFK2 adenoviral infection on CPCs are shown. *A*, representative fluorescence images of WT CPCs transduced with Ad-GFP or Ad-pd-PFK2 virus (100 MOI). *Scale bars*, 400 μm. *B*, representative Western blot of the pd-PFK2 enzyme in CPCs. The mutant PFK2 isoform was detected using an anti-PFKFB1 antibody. *C*, ECAR trace of WT CPCs left untransduced (*black circles*) or transduced with 100 MOI of Ad-GFP (*open circles*) or Ad-pd-PFK2 (*gray squares*) virus. The plot is representative of three independent experiments. *D*, radiometric measurement of glycolytic flux in WT CPCs left untransduced (*CTRL*) or transduced with Ad-GFP or Ad-pd-PFK2 viruses. The results represent three replicates/group. ***, $p \leq 0.001$ *versus* untransduced (*CTRL*); ##, $p \leq 0.01$ *versus* Ad-GFP. *E*, mitochondrial activity of WT CPCs left untransduced (*CTRL*) or transduced with Ad-GFP or Ad-pd-PFK2 viruses. The OCR is shown as a percentage of baseline to demonstrate the effects of glycolysis on mitochondrial activity upon exposure to glucose (*Glc*). The plot represents three independent experiments. *F*, proliferation of WT CPCs transduced with Ad-GFP or Ad-pd-PFK2 viruses. The cells were transduced with virus, and after 48 h, equal numbers of the cells were seeded. After an additional 48 h, the number of cells in each well was counted. The plot represents three independent experiments. *, $p \leq 0.05$; **, $p \leq 0.01$ *versus* untransduced (*CTRL*) and/or Ad-GFP.

thesis of lipids, nucleotides, and amino acids required for cell growth, viability, and differentiation (83–88). Thus, these pathways interconvert metabolites of sugar to the building blocks required for cell growth and function (89). Enzymatic reactions in the glycolytic pathway appear to coordinate flux through these collateral pathways. For example, PFK activity has been shown to regulate PPP flux in several cell types, which influences their proliferative capacity and sensitivity to oxidative stress (55–57, 90). In our study, lower flux of glucose carbon into the PPP in diabetic CPCs can be explained by an uncoupling of glycolysis, caused by elevated PFKFB3 levels, which could directly contribute to changes in cell competence. Our data suggest that, in CPCs, PFK activation quickly utilizes the glycolytic intermediates glucose-6-phosphate and F6P, thereby channeling glucose-derived carbons to the payoff phase (91) of glycolysis and to those ancillary pathways that utilize 3-carbon intermediates (*e.g.* the GLP). These results are consistent with previous studies showing that dysregulation of the PPP dimin-

ishes proliferation and survival of CPCs isolated from T1D mice (92).

Our studies suggest that diabetic CPCs are poised to differentiate into a preadipogenic phenotype. This is consistent with previous studies showing that hyperglycemia can promote adipogenic differentiation of muscle-derived stem cells (27). Interestingly, cardiac-derived cells with a mesenchymal phenotype are capable of differentiating into an adipocyte lineage *in vivo* (22, 93), and fibroadiposis has been suggested to be a disease of CPCs "gone awry" that occurs when they differentiate into adipocytes (94). With respect to diabetes, hyperglycemia has been shown to decrease the activity of GAPDH, which metabolizes GAP to 3-phosphoglycerate. This increases upstream metabolites, which could then flood ancillary pathways with glucose-derived carbon (67). Because CPCs have little gluconeogenic capacity, a hyperglycolytic phenotype may render the GLP as the primary ancillary pathway in diabetic CPCs that would be flooded because of excessive GAP and dihydroxyacetone phosphate (DHAP) accumulation. These metabolites and GLP activity likely play a role in instigating a preadipogenic phenotype in CPCs. Our stable isotope tracing data suggest that high levels of PFKFB3 would increase DHAP formation, which, in addition to providing glycerol for esterifying fatty acids, could trigger the adipogenic differentiation program by activating protein kinase C (27).

To study metabolic changes in diabetic cells, we developed a new approach to quantify changes in the coupling of flux between metabolic pathways using stable isotope tracing techniques. Typically, coupling refers to a connection between two things or systems. In biology, a typical example is mitochondrial (un)coupling, which is the relative (dis)connection of proton dislocation (caused by electron flow through the respiratory chain) with ATP production via mitochondrial ATP synthase. In the current context, we invoke the use of "coupling" to define metabolic pathway coupling, where the fluxes of metabolic pathways are in a certain proportion to that of other pathways in the network. In stable isotope metabolomics, the unique isotopologue patterns of metabolic products, which reflect the biological and biochemical history of the metabolites, leads to exact pathway assignment and assessment of relative changes in flux through known metabolic pathways. Our approach integrates this methodology and allows calculation of novel coupling quotients that have the potential to help identify the sites of metabolic uncoupling and to quantify the degree by which biochemical pathways are (un)coupled. Because metabolic flux configurations are a material cause of the catabolic and anabolic activities in cells and tissues (which, in turn, regulate the atomic composition and structural arrangement of the biological system), describing and quantifying metabolic pathways relative to one another could facilitate a quantitative evaluation of the metabolic network in an organism and could explain biological processes that cause diabetes and other diseases with a metabolic basis, such as aging.

In summary, our studies support the hypothesis that diabetes impairs CPC competence by uncoupling ancillary biosynthetic pathways of glucose metabolism. This hypothesis has both predictive and explanatory power. Specifically, our results support the notion that sustained up-regulation of PFKFB3 increases glycolytic rate in CPCs and causes disproportionate partitioning of glucose carbons into the PPP and GLP. The higher glycolytic phenotype appears to diminish their mitochondrial activity and proliferative capacity and could decrease their ability to survive and differentiate. We define a novel method to quantify metabolic pathway coupling in cells, which could be used to obtain new information on how the metabolic network changes with development, aging, and metabolic disease. This information could be useful for predicting the relative competence of cells destined for transplantation and would enable identification of loci responsible for metabolic dysfunction in diseased cells.

Author Contributions—J. K. S., P. K. L., and P. M. were responsible for concept and design, experimental studies, and data analysis and interpretation; A. A. G. was responsible for mutant PFK2 studies; P. H. was responsible for experimental studies and data analysis and interpretation; K. U. H. helped with mutant PFK2 constructs; X. W. was responsible for data analysis; X. Z. was responsible for use of core facilities; Q. L. was responsible for provision of study material; M. W. helped with experimental studies; R. B. and A. B. were responsible for financial support and concept and design; and B. G. H. was responsible for financial support, concept and design, assembly of data, data analysis and interpretation, and manuscript writing. All authors read and approved the final manuscript.

Acknowledgment—We thank Dr. Paul N. Epstein for providing plasmids containing the mutant PFK2 gene.

References

1. Wollert, K. C., Meyer, G. P., Lotz, J., Ringes-Lichtenberg, S., Lippolt, P., Breidenbach, C., Fichtner, S., Korte, T., Hornig, B., Messinger, D., Arseniev, L., Hertenstein, B., Ganser, A., and Drexler, H. (2004) Intracoronary autologous bone-marrow cell transfer after myocardial infarction: the BOOST randomised controlled clinical trial. *Lancet* **364,** 141–148
2. Schächinger, V., Erbs, S., Elsässer, A., Haberbosch, W., Hambrecht, R., Hölschermann, H., Yu, J., Corti, R., Mathey, D. G., Hamm, C. W., Süselbeck, T., Assmus, B., Tonn, T., Dimmeler, S., Zeiher, A. M., *et al.* (2006) Intracoronary bone marrow-derived progenitor cells in acute myocardial infarction. *N. Engl. J. Med.* **355,** 1210–1221
3. Hare, J. M., Fishman, J. E., Gerstenblith, G., DiFede Velazquez, D. L., Zambrano, J. P., Suncion, V. Y., Tracy, M., Ghersin, E., Johnston, P. V., Brinker, J. A., Breton, E., Davis-Sproul, J., Schulman, I. H., Byrnes, J., Mendizabal, A. M., *et al.* (2012) Comparison of allogeneic vs autologous bone marrow-derived mesenchymal stem cells delivered by transendocardial injection in patients with ischemic cardiomyopathy: the POSEIDON randomized trial. *JAMA* **308,** 2369–2379
4. Williams, A. R., Trachtenberg, B., Velazquez, D. L., McNiece, I., Altman, P., Rouy, D., Mendizabal, A. M., Pattany, P. M., Lopera, G. A., Fishman, J., Zambrano, J. P., Heldman, A. W., and Hare, J. M. (2011) Intramyocardial stem cell injection in patients with ischemic cardiomyopathy: functional recovery and reverse remodeling. *Circ. Res.* **108,** 792–796
5. Bolli, R., Chugh, A. R., D'Amario, D., Loughran, J. H., Stoddard, M. F., Ikram, S., Beache, G. M., Wagner, S. G., Leri, A., Hosoda, T., Sanada, F., Elmore, J. B., Goichberg, P., Cappetta, D., Solankhi, N. K., *et al.* (2011) Cardiac stem cells in patients with ischaemic cardiomyopathy (SCIPIO): initial results of a randomised phase 1 trial. *Lancet* **378,** 1847–1857
6. Chugh, A. R., Beache, G. M., Loughran, J. H., Mewton, N., Elmore, J. B., Kajstura, J., Pappas, P., Tatooles, A., Stoddard, M. F., Lima, J. A., Slaughter, M. S., Anversa, P., and Bolli, R. (2012) Administration of cardiac stem cells in patients with ischemic cardiomyopathy: the SCIPIO trial: surgical aspects and interim analysis of myocardial function and viability by magnetic resonance. *Circulation* **126,** S54–64

7. Ellison, G. M., Vicinanza, C., Smith, A. J., Aquila, I., Leone, A., Waring, C. D., Henning, B. J., Stirparo, G. G., Papait, R., Scarfò, M., Agosti, V., Viglietto, G., Condorelli, G., Indolfi, C., Ottolenghi, S., *et al.* (2013) Adult c-kit(pos) cardiac stem cells are necessary and sufficient for functional cardiac regeneration and repair. *Cell* **154,** 827–842
8. van Berlo, J. H., Kanisicak, O., Maillet, M., Vagnozzi, R. J., Karch, J., Lin, S. C., Middleton, R. C., Marbán, E., and Molkentin, J. D. (2014) c-kit$^+$ cells minimally contribute cardiomyocytes to the heart. *Nature* **509,** 337–341
9. Fischer, K. M., Cottage, C. T., Wu, W., Din, S., Gude, N. A., Avitabile, D., Quijada, P., Collins, B. L., Fransioli, J., and Sussman, M. A. (2009) Enhancement of myocardial regeneration through genetic engineering of cardiac progenitor cells expressing Pim-1 kinase. *Circulation* **120,** 2077–2087
10. Zhang, L. X., DeNicola, M., Qin, X., Du, J., Ma, J., Tina Zhao, Y., Zhuang, S., Liu, P. Y., Wei, L., Qin, G., Tang, Y., and Zhao, T. C. (2014) Specific inhibition of HDAC4 in cardiac progenitor cells enhances myocardial repairs. *Am. J. Physiol. Cell Physiol.* **307,** C358–C372
11. Zakharova, L., Nural-Guvener, H., Feehery, L., Popovic, S., Nimlos, J., and Gaballa, M. A. (2014) Retrograde coronary vein infusion of cardiac explant-derived c-Kit$^+$ cells improves function in ischemic heart failure. *J. Heart Lung Transplant.* **33,** 644–653
12. Bolli, R., Tang, X. L., Sanganalmath, S. K., Rimoldi, O., Mosna, F., Abdel-Latif, A., Jneid, H., Rota, M., Leri, A., and Kajstura, J. (2013) Intracoronary delivery of autologous cardiac stem cells improves cardiac function in a porcine model of chronic ischemic cardiomyopathy. *Circulation* **128,** 122–131
13. Dawn, B., Stein, A. B., Urbanek, K., Rota, M., Whang, B., Rastaldo, R., Torella, D., Tang, X. L., Rezazadeh, A., Kajstura, J., Leri, A., Hunt, G., Varma, J., Prabhu, S. D., Anversa, P., *et al.* (2005) Cardiac stem cells delivered intravascularly traverse the vessel barrier, regenerate infarcted myocardium, and improve cardiac function. *Proc. Natl. Acad. Sci. U.S.A.* **102,** 3766–3771
14. Welt, F. G., Gallegos, R., Connell, J., Kajstura, J., D'Amario, D., Kwong, R. Y., Coelho-Filho, O., Shah, R., Mitchell, R., Leri, A., Foley, L., Anversa, P., and Pfeffer, M. A. (2013) Effect of cardiac stem cells on left-ventricular remodeling in a canine model of chronic myocardial infarction. *Circ. Heart Fail.* **6,** 99–106
15. Agoston, I., Cameron, C. S., Yao, D., Dela Rosa, A., Mann, D. L., and Deswal, A. (2004) Comparison of outcomes of white versus black patients hospitalized with heart failure and preserved ejection fraction. *Am. J. Cardiol.* **94,** 1003–1007
16. Rathore, S. S., Foody, J. M., Wang, Y., Smith, G. L., Herrin, J., Masoudi, F. A., Wolfe, P., Havranek, E. P., Ordin, D. L., and Krumholz, H. M. (2003) Race, quality of care, and outcomes of elderly patients hospitalized with heart failure. *JAMA* **289,** 2517–2524
17. Singh, H., Gordon, H. S., and Deswal, A. (2005) Variation by race in factors contributing to heart failure hospitalizations. *J. Card. Fail.* **11,** 23–29
18. Rota, M., LeCapitaine, N., Hosoda, T., Boni, A., De Angelis, A., Padin-Iruegas, M. E., Esposito, G., Vitale, S., Urbanek, K., Casarsa, C., Giorgio, M., Lüscher, T. F., Pelicci, P. G., Anversa, P., Leri, A., *et al.* (2006) Diabetes promotes cardiac stem cell aging and heart failure, which are prevented by deletion of the p66shc gene. *Circ. Res.* **99,** 42–52
19. Molgat, A. S., Tilokee, E. L., Rafatian, G., Vulesevic, B., Ruel, M., Milne, R., Suuronen, E. J., and Davis, D. R. (2014) Hyperglycemia inhibits cardiac stem cell-mediated cardiac repair and angiogenic capacity. *Circulation* **130,** S70–76
20. Vasa, M., Fichtlscherer, S., Aicher, A., Adler, K., Urbich, C., Martin, H., Zeiher, A. M., and Dimmeler, S. (2001) Number and migratory activity of circulating endothelial progenitor cells inversely correlate with risk factors for coronary artery disease. *Circ. Res.* **89,** E1–E7
21. Saito, H., Yamamoto, Y., and Yamamoto, H. (2012) Diabetes alters subsets of endothelial progenitor cells that reside in blood, bone marrow, and spleen. *Am. J. Physiol. Cell Physiol.* **302,** C892–C901
22. Yan, J., Tie, G., Wang, S., Messina, K. E., DiDato, S., Guo, S., and Messina, L. M. (2012) Type 2 diabetes restricts multipotency of mesenchymal stem cells and impairs their capacity to augment postischemic neovascularization in db/db mice. *J. Am. Heart Assoc.* **1,** e002238
23. Yiu, K. H., and Tse, H. F. (2014) Specific role of impaired glucose metabolism and diabetes mellitus in endothelial progenitor cell characteristics and function. *Arterioscler. Thromb. Vasc. Biol.* **34,** 1136–1143
24. Albiero, M., Poncina, N., Tjwa, M., Ciciliot, S., Menegazzo, L., Ceolotto, G., Vigili de Kreutzenberg, S., Moura, R., Giorgio, M., Pelicci, P., Avogaro, A., and Fadini, G. P. (2014) Diabetes causes bone marrow autonomic neuropathy and impairs stem cell mobilization via dysregulated p66Shc and Sirt1. *Diabetes* **63,** 1353–1365
25. Tepper, O. M., Galiano, R. D., Capla, J. M., Kalka, C., Gagne, P. J., Jacobowitz, G. R., Levine, J. P., and Gurtner, G. C. (2002) Human endothelial progenitor cells from type II diabetics exhibit impaired proliferation, adhesion, and incorporation into vascular structures. *Circulation* **106,** 2781–2786
26. Ferraro, F., Lymperi, S., Méndez-Ferrer, S., Saez, B., Spencer, J. A., Yeap, B. Y., Masselli, E., Graiani, G., Prezioso, L., Rizzini, E. L., Mangoni, M., Rizzoli, V., Sykes, S. M., Lin, C. P., Frenette, P. S., *et al.* (2011) Diabetes impairs hematopoietic stem cell mobilization by altering niche function. *Sci. Transl. Med.* **3,** 104ra101
27. Aguiari, P., Leo, S., Zavan, B., Vindigni, V., Rimessi, A., Bianchi, K., Franzin, C., Cortivo, R., Rossato, M., Vettor, R., Abatangelo, G., Pozzan, T., Pinton, P., and Rizzuto, R. (2008) High glucose induces adipogenic differentiation of muscle-derived stem cells. *Proc. Natl. Acad. Sci. U.S.A.* **105,** 1226–1231
28. Caballero, S., Sengupta, N., Afzal, A., Chang, K. H., Li Calzi, S., Guberski, D. L., Kern, T. S., and Grant, M. B. (2007) Ischemic vascular damage can be repaired by healthy, but not diabetic, endothelial progenitor cells. *Diabetes* **56,** 960–967
29. Li, Q., Guo, Y., Ou, Q., Chen, N., Wu, W. J., Yuan, F., O'Brien, E., Wang, T., Luo, L., Hunt, G. N., Zhu, X., and Bolli, R. (2011) Intracoronary administration of cardiac stem cells in mice: a new, improved technique for cell therapy in murine models. *Basic Res. Cardiol.* **106,** 849–864
30. Zafir, A., Readnower, R., Long, B. W., McCracken, J., Aird, A., Alvarez, A., Cummins, T. D., Li, Q., Hill, B. G., Bhatnagar, A., Prabhu, S. D., Bolli, R., and Jones, S. P. (2013) Protein *O*-GlcNAcylation is a novel cytoprotective signal in cardiac stem cells. *Stem Cells* **31,** 765–775
31. Salabei, J. K., Lorkiewicz, P. K., Holden, C. R., Li, Q., Hong, K. U., Bolli, R., Bhatnagar, A., and Hill, B. G. (2015) Glutamine regulates cardiac progenitor cell metabolism and proliferation. *Stem Cells* **33,** 2613–2627
32. Fransioli, J., Bailey, B., Gude, N. A., Cottage, C. T., Muraski, J. A., Emmanuel, G., Wu, W., Alvarez, R., Rubio, M., Ottolenghi, S., Schaefer, E., and Sussman, M. A. (2008) Evolution of the c-kit-positive cell response to pathological challenge in the myocardium. *Stem Cells* **26,** 1315–1324
33. Mohsin, S., Khan, M., Toko, H., Bailey, B., Cottage, C. T., Wallach, K., Nag, D., Lee, A., Siddiqi, S., Lan, F., Fischer, K. M., Gude, N., Quijada, P., Avitabile, D., Truffa, S., *et al.* (2012) Human cardiac progenitor cells engineered with Pim-I kinase enhance myocardial repair. *J. Am. Coll. Cardiol.* **60,** 1278–1287
34. Beltrami, A. P., Barlucchi, L., Torella, D., Baker, M., Limana, F., Chimenti, S., Kasahara, H., Rota, M., Musso, E., Urbanek, K., Leri, A., Kajstura, J., Nadal-Ginard, B., and Anversa, P. (2003) Adult cardiac stem cells are multipotent and support myocardial regeneration. *Cell* **114,** 763–776
35. Hill, B. G., Dranka, B. P., Zou, L., Chatham, J. C., and Darley-Usmar, V. M. (2009) Importance of the bioenergetic reserve capacity in response to cardiomyocyte stress induced by 4-hydroxynonenal. *Biochem. J.* **424,** 99–107
36. Cummins, T. D., Holden, C. R., Sansbury, B. E., Gibb, A. A., Shah, J., Zafar, N., Tang, Y., Hellmann, J., Rai, S. N., Spite, M., Bhatnagar, A., and Hill, B. G. (2014) Metabolic remodeling of white adipose tissue in obesity. *Am. J. Physiol. Endocrinol. Metab.* **307,** E262–E277
37. Tauler, A., Lin, K., and Pilkis, S. J. (1990) Hepatic 6-phosphofructo-2-kinase/fructose-2,6-bisphosphatase. Use of site-directed mutagenesis to evaluate the roles of His-258 and His-392 in catalysis. *J. Biol. Chem.* **265,** 15617–15622
38. Kurland, I. J., el-Maghrabi, M. R., Correia, J. J., and Pilkis, S. J. (1992) Rat liver 6-phosphofructo-2-kinase/fructose-2,6-bisphosphatase. Properties of phospho- and dephospho-forms and of two mutants in which Ser32 has been changed by site-directed mutagenesis. *J. Biol. Chem.* **267,** 4416–4423
39. Argaud, D., Lange, A. J., Becker, T. C., Okar, D. A., el-Maghrabi, M. R.,

Newgard, C. B., and Pilkis, S. J. (1995) Adenovirus-mediated overexpression of liver 6-phosphofructo-2-kinase/fructose-2,6-bisphosphatase in gluconeogenic rat hepatoma cells. Paradoxical effect on Fru-2,6-P2 levels. *J. Biol. Chem.* **270,** 24229–24236
40. Wang, Q., Donthi, R. V., Wang, J., Lange, A. J., Watson, L. J., Jones, S. P., and Epstein, P. N. (2008) Cardiac phosphatase-deficient 6-phosphofructo-2-kinase/fructose-2,6-bisphosphatase increases glycolysis, hypertrophy, and myocyte resistance to hypoxia. *Am. J. Physiol. Heart. Circ. Physiol.* **294,** H2889–H2897
41. Ashcroft, S. J., Weerasinghe, L. C., Bassett, J. M., and Randle, P. J. (1972) The pentose cycle and insulin release in mouse pancreatic islets. *Biochem. J.* **126,** 525–532
42. Le, A., Lane, A. N., Hamaker, M., Bose, S., Gouw, A., Barbi, J., Tsukamoto, T., Rojas, C. J., Slusher, B. S., Zhang, H., Zimmerman, L. J., Liebler, D. C., Slebos, R. J., Lorkiewicz, P. K., Higashi, R. M., *et al.* (2012) Glucose-independent glutamine metabolism via TCA cycling for proliferation and survival in B cells. *Cell Metab.* **15,** 110–121
43. Lorkiewicz, P., Higashi, R. M., Lane, A. N., and Fan, T. W. (2012) High information throughput analysis of nucleotides and their isotopically enriched isotopologues by direct-infusion FTICR-MS. *Metabolomics* **8,** 930–939
44. Lane, A. N., Fan, T. W., Xie, Z., Moseley, H. N., and Higashi, R. M. (2009) Isotopomer analysis of lipid biosynthesis by high resolution mass spectrometry and NMR. *Anal. Chim. Acta* **651,** 201–208
45. Hsu, Y. C., Li, L., and Fuchs, E. (2014) Transit-amplifying cells orchestrate stem cell activity and tissue regeneration. *Cell* **157,** 935–949
46. Gupta, R. K., Mepani, R. J., Kleiner, S., Lo, J. C., Khandekar, M. J., Cohen, P., Frontini, A., Bhowmick, D. C., Ye, L., Cinti, S., and Spiegelman, B. M. (2012) Zfp423 expression identifies committed preadipocytes and localizes to adipose endothelial and perivascular cells. *Cell Metab.* **15,** 230–239
47. Huang, H., Song, T. J., Li, X., Hu, L., He, Q., Liu, M., Lane, M. D., and Tang, Q. Q. (2009) BMP signaling pathway is required for commitment of C3H10T1/2 pluripotent stem cells to the adipocyte lineage. *Proc. Natl. Acad. Sci. U.S.A.* **106,** 12670–12675
48. Huang, H. Y., Hu, L. L., Song, T. J., Li, X., He, Q., Sun, X., Li, Y. M., Lu, H. J., Yang, P. Y., and Tang, Q. Q. (2011) Involvement of cytoskeleton-associated proteins in the commitment of C3H10T1/2 pluripotent stem cells to adipocyte lineage induced by BMP2/4. *Mol. Cell. Proteomics* **10,** M110.002691
49. Huang, H. Y., Chen, S. Z., Zhang, W. T., Wang, S. S., Liu, Y., Li, X., Sun, X., Li, Y. M., Wen, B., Lei, Q. Y., and Tang, Q. Q. (2013) Induction of EMT-like response by BMP4 via up-regulation of lysyl oxidase is required for adipocyte lineage commitment. *Stem Cell Res.* **10,** 278–287
50. Zdychová, J., and Komers, R. (2005) Emerging role of Akt kinase/protein kinase B signaling in pathophysiology of diabetes and its complications. *Physiol. Res.* **54,** 1–16
51. Kim, Y. B., Shulman, G. I., and Kahn, B. B. (2002) Fatty acid infusion selectively impairs insulin action on Akt1 and protein kinase Cλ/ζ but not on glycogen synthase kinase-3. *J. Biol. Chem.* **277,** 32915–32922
52. Mookerjee, S. A., Goncalves, R. L., Gerencser, A. A., Nicholls, D. G., and Brand, M. D. (2015) The contributions of respiration and glycolysis to extracellular acid production. *Biochim. Biophys. Acta* **1847,** 171–181
53. Mor, I., Cheung, E. C., and Vousden, K. H. (2011) Control of glycolysis through regulation of PFK1: old friends and recent additions. *Cold Spring Harb. Symp. Quant. Biol.* **76,** 211–216
54. Yalcin, A., Telang, S., Clem, B., and Chesney, J. (2009) Regulation of glucose metabolism by 6-phosphofructo-2-kinase/fructose-2,6-bisphosphatases in cancer. *Exp. Mol. Pathol.* **86,** 174–179
55. Yi, W., Clark, P. M., Mason, D. E., Keenan, M. C., Hill, C., Goddard, W. A., 3rd, Peters, E. C., Driggers, E. M., and Hsieh-Wilson, L. C. (2012) Phosphofructokinase 1 glycosylation regulates cell growth and metabolism. *Science* **337,** 975–980
56. Boada, J., Roig, T., Perez, X., Gamez, A., Bartrons, R., Cascante, M., and Bermúdez, J. (2000) Cells overexpressing fructose-2,6-bisphosphatase showed enhanced pentose phosphate pathway flux and resistance to oxidative stress. *FEBS Lett.* **480,** 261–264
57. Yamamoto, T., Takano, N., Ishiwata, K., Ohmura, M., Nagahata, Y., Matsuura, T., Kamata, A., Sakamoto, K., Nakanishi, T., Kubo, A., Hishiki, T., and Suematsu, M. (2014) Reduced methylation of PFKFB3 in cancer cells shunts glucose towards the pentose phosphate pathway. *Nat. Commun.* **5,** 3480
58. Lorkiewicz, P., and Cecilia Yappert, M. (2009) 2-(2-aminoethylamino)-5-nitropyridine as a basic matrix for negative-mode matrix-assisted laser desorption/ionization analysis of phospholipids. *J Mass Spectrom.* **44,** 137–143
59. Sakakibara, R., Kato, M., Okamura, N., Nakagawa, T., Komada, Y., Tominaga, N., Shimojo, M., and Fukasawa, M. (1997) Characterization of a human placental fructose-6-phosphate, 2-kinase/fructose-2,6-bisphosphatase. *J. Biochem.* **122,** 122–128
60. Duran, J., Obach, M., Navarro-Sabate, A., Manzano, A., Gómez, M., Rosa, J. L., Ventura, F., Perales, J. C., and Bartrons, R. (2009) Pfkfb3 is transcriptionally upregulated in diabetic mouse liver through proliferative signals. *FEBS J.* **276,** 4555–4568
61. Clem, B., Telang, S., Clem, A., Yalcin, A., Meier, J., Simmons, A., Rasku, M. A., Arumugam, S., Dean, W. L., Eaton, J., Lane, A., Trent, J. O., and Chesney, J. (2008) Small-molecule inhibition of 6-phosphofructo-2-kinase activity suppresses glycolytic flux and tumor growth. *Mol. Cancer Ther.* **7,** 110–120
62. Telang, S., Clem, B. F., Klarer, A. C., Clem, A. L., Trent, J. O., Bucala, R., and Chesney, J. (2012) Small molecule inhibition of 6-phosphofructo-2-kinase suppresses T cell activation. *J. Transl. Med.* **10,** 95
63. Clem, B. F., O'Neal, J., Tapolsky, G., Clem, A. L., Imbert-Fernandez, Y., Kerr, D. A., 2nd, Klarer, A. C., Redman, R., Miller, D. M., Trent, J. O., Telang, S., and Chesney, J. (2013) Targeting 6-phosphofructo-2-kinase (PFKFB3) as a therapeutic strategy against cancer. *Mol. Cancer Ther.* **12,** 1461–1470
64. Chesney, J., and Telang, S. (2013) Regulation of glycolytic and mitochondrial metabolism by ras. *Curr. Pharm. Biotechnol.* **14,** 251–260
65. Yalcin, A., Clem, B. F., Simmons, A., Lane, A., Nelson, K., Clem, A. L., Brock, E., Siow, D., Wattenberg, B., Telang, S., and Chesney, J. (2009) Nuclear targeting of 6-phosphofructo-2-kinase (PFKFB3) increases proliferation via cyclin-dependent kinases. *J. Biol. Chem.* **284,** 24223–24232
66. Wu, C., Okar, D. A., Stoeckman, A. K., Peng, L. J., Herrera, A. H., Herrera, J. E., Towle, H. C., and Lange, A. J. (2004) A potential role for fructose-2,6-bisphosphate in the stimulation of hepatic glucokinase gene expression. *Endocrinology* **145,** 650–658
67. Giacco, F., and Brownlee, M. (2010) Oxidative stress and diabetic complications. *Circ. Res.* **107,** 1058–1070
68. Crabtree, H. G. (1929) Observations on the carbohydrate metabolism of tumours. *Biochem. J.* **23,** 536–545
69. Diaz-Ruiz, R., Rigoulet, M., and Devin, A. (2011) The Warburg and Crabtree effects: on the origin of cancer cell energy metabolism and of yeast glucose repression. *Biochim. Biophys. Acta* **1807,** 568–576
70. Chan, H. H., Meher Homji, Z., Gomes, R. S., Sweeney, D., Thomas, G. N., Tan, J. J., Zhang, H., Perbellini, F., Stuckey, D. J., Watt, S. M., Taggart, D., Clarke, K., Martin-Rendon, E., and Carr, C. A. (2012) Human cardiosphere-derived cells from patients with chronic ischaemic heart disease can be routinely expanded from atrial but not epicardial ventricular biopsies. *J. Cardiovasc. Transl. Res.* **5,** 678–687
71. Cheng, K., Ibrahim, A., Hensley, M. T., Shen, D., Sun, B., Middleton, R., Liu, W., Smith, R. R., and Marbán, E. (2014) Relative roles of CD90 and c-kit to the regenerative efficacy of cardiosphere-derived cells in humans and in a mouse model of myocardial infarction. *J. Am. Heart Assoc.* **3,** e001260
72. Atsumi, T., Nishio, T., Niwa, H., Takeuchi, J., Bando, H., Shimizu, C., Yoshioka, N., Bucala, R., and Koike, T. (2005) Expression of inducible 6-phosphofructo-2-kinase/fructose-2,6-bisphosphatase/PFKFB3 isoforms in adipocytes and their potential role in glycolytic regulation. *Diabetes* **54,** 3349–3357
73. Huo, Y., Guo, X., Li, H., Wang, H., Zhang, W., Wang, Y., Zhou, H., Gao, Z., Telang, S., Chesney, J., Chen, Y. E., Ye, J., Chapkin, R. S., and Wu, C. (2010) Disruption of inducible 6-phosphofructo-2-kinase ameliorates diet-induced adiposity but exacerbates systemic insulin resistance and adipose tissue inflammatory response. *J. Biol. Chem.* **285,** 3713–3721
74. Cordero-Espinoza, L., and Hagen, T. (2013) Increased concentrations of fructose 2,6-bisphosphate contribute to the Warburg effect in phospha-

tase and tensin homolog (PTEN)-deficient cells. *J. Biol. Chem.* **288,** 36020–36028
75. Trefely, S., Khoo, P. S., Krycer, J. R., Chaudhuri, R., Fazakerley, D. J., Parker, B. L., Sultani, G., Lee, J., Stephan, J. P., Torres, E., Jung, K., Kuijl, C., James, D. E., Junutula, J. R., and Stöckli, J. (2015) Kinome screen identifies PFKFB3 and glucose metabolism as important regulators of the insulin/insulin-like growth factor (IGF)-1 signaling pathway. *J. Biol. Chem.* **290,** 25834–25846
76. Hubbard, S. R. (2013) The insulin receptor: both a prototypical and atypical receptor tyrosine kinase. *Cold Spring Harb. Perspect. Biol.* **5,** a008946
77. De Saedeleer, C. J., Copetti, T., Porporato, P. E., Verrax, J., Feron, O., and Sonveaux, P. (2012) Lactate activates HIF-1 in oxidative but not in Warburg-phenotype human tumor cells. *PLoS One* **7,** e46571
78. Ruan, G. X., and Kazlauskas, A. (2013) Lactate engages receptor tyrosine kinases Axl, Tie2, and vascular endothelial growth factor receptor 2 to activate phosphoinositide 3-kinase/Akt and promote angiogenesis. *J. Biol. Chem.* **288,** 21161–21172
79. Ahmed, K., Tunaru, S., Tang, C., Müller, M., Gille, A., Sassmann, A., Hanson, J., and Offermanns, S. (2010) An autocrine lactate loop mediates insulin-dependent inhibition of lipolysis through GPR81. *Cell Metab.* **11,** 311–319
80. Cheng, Z., Tseng, Y., and White, M. F. (2010) Insulin signaling meets mitochondria in metabolism. *Trends Endocrinol. Metab.* **21,** 589–598
81. Sundaresan, N. R., Pillai, V. B., Wolfgeher, D., Samant, S., Vasudevan, P., Parekh, V., Raghuraman, H., Cunningham, J. M., Gupta, M., and Gupta, M. P. (2011) The deacetylase SIRT1 promotes membrane localization and activation of Akt and PDK1 during tumorigenesis and cardiac hypertrophy. *Sci. Signal.* **4,** ra46
82. Park, S. Y., Ryu, J., and Lee, W. (2005) *O*-GlcNAc modification on IRS-1 and Akt2 by PUGNAc inhibits their phosphorylation and induces insulin resistance in rat primary adipocytes. *Exp. Mol. Med.* **37,** 220–229
83. van Heerden, J. H., Wortel, M. T., Bruggeman, F. J., Heijnen, J. J., Bollen, Y. J., Planqué, R., Hulshof, J., O'Toole, T. G., Wahl, S. A., and Teusink, B. (2014) Lost in transition: start-up of glycolysis yields subpopulations of nongrowing cells. *Science* **343,** 1245114
84. Stelling, J., Sauer, U., Szallasi, Z., Doyle, F. J., 3rd, and Doyle, J. (2004) Robustness of cellular functions. *Cell* **118,** 675–685
85. Teusink, B., Walsh, M. C., van Dam, K., and Westerhoff, H. V. (1998) The danger of metabolic pathways with turbo design. *Trends Biochem. Sci.* **23,** 162–169
86. Ito, K., and Suda, T. (2014) Metabolic requirements for the maintenance of self-renewing stem cells. *Nat. Rev. Mol. Cell Biol.* **15,** 243–256
87. Panopoulos, A. D., Yanes, O., Ruiz, S., Kida, Y. S., Diep, D., Tautenhahn, R., Herrerías, A., Batchelder, E. M., Plongthongkum, N., Lutz, M., Berggren, W. T., Zhang, K., Evans, R. M., Siuzdak, G., and Izpisua Belmonte, J. C. (2012) The metabolome of induced pluripotent stem cells reveals metabolic changes occurring in somatic cell reprogramming. *Cell Res.* **22,** 168–177
88. Vacanti, N. M., and Metallo, C. M. (2013) Exploring metabolic pathways that contribute to the stem cell phenotype. *Biochim. Biophys. Acta* **1830,** 2361–2369
89. Noor, E., Eden, E., Milo, R., and Alon, U. (2010) Central carbon metabolism as a minimal biochemical walk between precursors for biomass and energy. *Mol. Cell* **39,** 809–820
90. Blackmore, P. F., and Shuman, E. A. (1982) Regulation of hepatic altro heptulose 1,7-bisphosphate levels and control of flux through the pentose pathway by fructose 2,6-bisphosphate. *FEBS Lett.* **142,** 255–259
91. Lehninger, A. L., Nelson, D. L., and Cox, M. M. (2000) Chapter 15. In: *Lehninger Principles of Biochemistry*, 3rd ed., pp. 527–566, Worth Publishers, New York
92. Katare, R., Oikawa, A., Cesselli, D., Beltrami, A. P., Avolio, E., Muthukrishnan, D., Munasinghe, P. E., Angelini, G., Emanueli, C., and Madeddu, P. (2013) Boosting the pentose phosphate pathway restores cardiac progenitor cell availability in diabetes. *Cardiovasc. Res.* **97,** 55–65
93. Lombardi, R., Dong, J., Rodriguez, G., Bell, A., Leung, T. K., Schwartz, R. J., Willerson, J. T., Brugada, R., and Marian, A. J. (2009) Genetic fate mapping identifies second heart field progenitor cells as a source of adipocytes in arrhythmogenic right ventricular cardiomyopathy. *Circ. Res.* **104,** 1076–1084
94. Lombardi, R., and Marian, A. J. (2011) Molecular genetics and pathogenesis of arrhythmogenic right ventricular cardiomyopathy: a disease of cardiac stem cells. *Pediatr. Cardiol.* **32,** 360–365